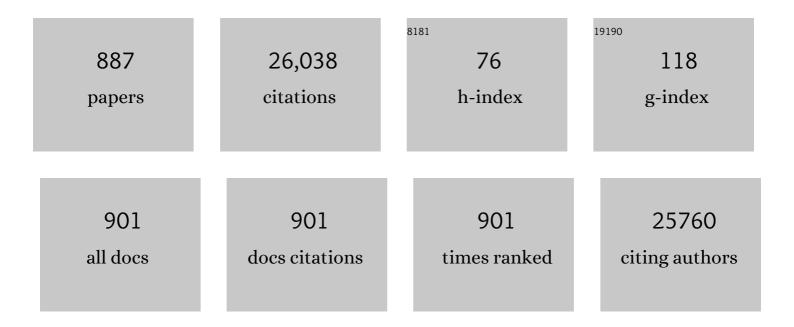
List of Publications by Year in descending order

Source: https://exaly.com/author-pdf/3231072/publications.pdf Version: 2024-02-01



DEPEN YANC

#	Article	IF	CITATIONS
1	Low Temperature Synthesis of Flowerlike ZnO Nanostructures by Cetyltrimethylammonium Bromide-Assisted Hydrothermal Process. Journal of Physical Chemistry B, 2004, 108, 3955-3958.	2.6	484
2	Synthesis of Pdâ^'Pt Bimetallic Nanocrystals with a Concave Structure through a Bromide-Induced Galvanic Replacement Reaction. Journal of the American Chemical Society, 2011, 133, 6078-6089.	13.7	405
3	Intermetallic Nanocrystals: Syntheses and Catalytic Applications. Advanced Materials, 2017, 29, 1605997.	21.0	375
4	Controllable Growth of ZnO Microcrystals by a Capping-Molecule-Assisted Hydrothermal Process. Crystal Growth and Design, 2005, 5, 547-550.	3.0	320
5	Luminescent Metal–Organic Framework Films As Highly Sensitive and Fast-Response Oxygen Sensors. Journal of the American Chemical Society, 2014, 136, 5527-5530.	13.7	319
6	Enhanced Electronic Properties of SnO <sub>2</sub> <i>via</i> Electron Transfer from Graphene Quantum Dots for Efficient Perovskite Solar Cells. ACS Nano, 2017, 11, 9176-9182.	14.6	302
7	Selective etching of GaN polar surface in potassium hydroxide solution studied by x-ray photoelectron spectroscopy. Journal of Applied Physics, 2001, 90, 4219-4223.	2.5	301
8	Synthesis of flower-like ZnO nanostructures by an organic-free hydrothermal process. Nanotechnology, 2004, 15, 622-626.	2.6	290
9	Plasmonic Silicon Quantum Dots Enabled High-Sensitivity Ultrabroadband Photodetection of Graphene-Based Hybrid Phototransistors. ACS Nano, 2017, 11, 9854-9862.	14.6	285
10	Facile Synthesis of Pd–Pt Alloy Nanocages and Their Enhanced Performance for Preferential Oxidation of CO in Excess Hydrogen. ACS Nano, 2011, 5, 8212-8222.	14.6	236
11	Large-Scale Synthesis of SnO2 Nanotube Arrays as High-Performance Anode Materials of Li-Ion Batteries. Journal of Physical Chemistry C, 2011, 115, 11302-11305.	3.1	231
12	Demonstration of optical microfiber knot resonators. Applied Physics Letters, 2006, 88, 223501.	3.3	227
13	A self-powered high-performance graphene/silicon ultraviolet photodetector with ultra-shallow junction: breaking the limit of silicon?. Npj 2D Materials and Applications, 2017, 1, .	7.9	211
14	Graphene Coupled with Silicon Quantum Dots for Highâ€Performance Bulkâ€Siliconâ€Based Schottkyâ€Junction Photodetectors. Advanced Materials, 2016, 28, 4912-4919.	21.0	206
15	A simple hydrothermal route for synthesizing SnO2quantum dots. Nanotechnology, 2006, 17, 2386-2389.	2.6	202
16	Epitaxial Growth of Twinned Au–Pt Core–Shell Star-Shaped Decahedra as Highly Durable Electrocatalysts. Nano Letters, 2015, 15, 7808-7815.	9.1	195
17	Controlling the Morphology of Rhodium Nanocrystals by Manipulating the Growth Kinetics with a Syringe Pump. Nano Letters, 2011, 11, 898-903.	9.1	190
18	Porous ZnCo <sub>2</sub> O <sub>4</sub> Nanowires Synthesis via Sacrificial Templates: High-Performance Anode Materials of Li-Ion Batteries. Inorganic Chemistry, 2011, 50, 3320-3324.	4.0	178

#	Article	IF	CITATIONS
19	Multiwalled Carbon Nanotubes Anchored with SnS <sub>2</sub> Nanosheets as High-Performance Anode Materials of Lithium-Ion Batteries. ACS Applied Materials & Interfaces, 2011, 3, 4067-4074.	8.0	159
20	Enhancement of ZnO light emission via coupling with localized surface plasmon of Ag island film. Applied Physics Letters, 2008, 92, .	3.3	156
21	A selective NH3 gas sensor based on Fe2O3–ZnO nanocomposites at room temperature. Sensors and Actuators B: Chemical, 2006, 114, 910-915.	7.8	155
22	Broadband optoelectronic synaptic devices based on silicon nanocrystals for neuromorphic computing. Nano Energy, 2018, 52, 422-430.	16.0	150
23	Seed-assisted cast quasi-single crystalline silicon for photovoltaic application: Towards high efficiency and low cost silicon solar cells. Solar Energy Materials and Solar Cells, 2012, 101, 95-101.	6.2	146
24	Optoelectronic Synaptic Devices for Neuromorphic Computing. Advanced Intelligent Systems, 2021, 3, 2000099.	6.1	143
25	Engineering crystalline structures of two-dimensional MoS <sub>2</sub> sheets for high-performance organic solar cells. Journal of Materials Chemistry A, 2014, 2, 7727-7733.	10.3	142
26	Kinetically controlled synthesis of Pt–Cu alloy concave nanocubes with high-index facets for methanol electro-oxidation. Chemical Communications, 2014, 50, 560-562.	4.1	140
27	CNTs@SnO <sub>2</sub> @C Coaxial Nanocables with Highly Reversible Lithium Storage. Journal of Physical Chemistry C, 2010, 114, 22535-22538.	3.1	139
28	Controllable growth of ZnO nanostructures by citric acid assisted hydrothermal process. Materials Letters, 2005, 59, 1696-1700.	2.6	138
29	Ligand-free Self-Assembly of Ceria Nanocrystals into Nanorods by Oriented Attachment at Low Temperature. Journal of Physical Chemistry C, 2007, 111, 12677-12680.	3.1	137
30	Comparative Study on the Localized Surface Plasmon Resonance of Boron- and Phosphorus-Doped Silicon Nanocrystals. ACS Nano, 2015, 9, 378-386.	14.6	133
31	Carbon-coated SnO <sub>2</sub> nanotubes: template-engaged synthesis and their application in lithium-ion batteries. Nanoscale, 2011, 3, 746-750.	5.6	131
32	Electrically pumped ZnO film ultraviolet random lasers on silicon substrate. Applied Physics Letters, 2007, 91, .	3.3	126
33	Photoluminescence of Si-rich silicon nitride: Defect-related states and silicon nanoclusters. Applied Physics Letters, 2007, 90, 131903.	3.3	124
34	CuO nanodendrites synthesized by a novel hydrothermal route. Nanotechnology, 2004, 15, 1428-1432.	2.6	122
35	Optically Stimulated Synaptic Devices Based on the Hybrid Structure of Silicon Nanomembrane and Perovskite. Nano Letters, 2020, 20, 3378-3387.	9.1	121
36	In situ Study of Oxidative Etching of Palladium Nanocrystals by Liquid Cell Electron Microscopy. Nano Letters, 2014, 14, 3761-3765.	9.1	120

#	Article	IF	CITATIONS
37	Enhancing the Efficiency of Multicrystalline Silicon Solar Cells by the Inkjet Printing of Silicon-Quantum-Dot Ink. Journal of Physical Chemistry C, 2012, 116, 21240-21243.	3.1	119
38	Ultraviolet electroluminescence from ZnOâ^•p‣i heterojunctions. Journal of Applied Physics, 2007, 101, 053103.	2.5	117
39	Spin-coating silicon-quantum-dot ink to improve solar cell efficiency. Solar Energy Materials and Solar Cells, 2011, 95, 2941-2945.	6.2	117
40	Nanocrystals Composed of Alternating Shells of Pd and Pt Can Be Obtained by Sequentially Adding Different Precursors. Journal of the American Chemical Society, 2011, 133, 10422-10425.	13.7	115
41	Thin Czochralski silicon solar cells based on diamond wire sawing technology. Solar Energy Materials and Solar Cells, 2012, 98, 337-342.	6.2	115
42	Coupling PtNi Ultrathin Nanowires with MXenes for Boosting Electrocatalytic Hydrogen Evolution in Both Acidic and Alkaline Solutions. Small, 2019, 15, e1805474.	10.0	113
43	Arrays of ZnO nanowires fabricated by a simple chemical solution route. Nanotechnology, 2003, 14, 423-426.	2.6	111
44	Highly loaded CoO/graphene nanocomposites as lithium-ion anodes with superior reversible capacity. Journal of Materials Chemistry A, 2013, 1, 2337.	10.3	111
45	Synaptic silicon-nanocrystal phototransistors for neuromorphic computing. Nano Energy, 2019, 63, 103859.	16.0	107
46	From cobalt nitrate carbonate hydroxide hydrate nanowires to porous Co <sub>3</sub> O <sub>4</sub> nanorods for high performance lithium-ion battery electrodes. Nanotechnology, 2008, 19, 035711.	2.6	105
47	Selective Synthesis of Fe2O3 and Fe3O4 Nanowires Via a Single Precursor: A General Method for Metal Oxide Nanowires. Nanoscale Research Letters, 2010, 5, 1295-1300.	5.7	105
48	Hydrothermal Synthesis of Zn2SnO4 Nanorods in the Diameter Regime of Sub-5 nm and Their Properties. Journal of Physical Chemistry B, 2006, 110, 7631-7634.	2.6	104
49	Self-Templating Synthesis of SnO <sub>2</sub> –Carbon Hybrid Hollow Spheres for Superior Reversible Lithium Ion Storage. ACS Applied Materials & Interfaces, 2011, 3, 1946-1952.	8.0	104
50	Tuning Surface Structure and Strain in Pd–Pt Core–Shell Nanocrystals for Enhanced Electrocatalytic Oxygen Reduction. Small, 2017, 13, 1603423.	10.0	104
51	Enhancement and patterning of ultraviolet emission in ZnO with an electron beam. Applied Physics Letters, 2006, 88, 134103.	3.3	103
52	Gas sensing behavior of polyvinylpyrrolidone-modified ZnO nanoparticles for trimethylamine. Sensors and Actuators B: Chemical, 2006, 113, 324-328.	7.8	103
53	Epitaxial Growth of Multimetallic Pd@PtM (M = Ni, Rh, Ru) Core–Shell Nanoplates Realized by in Situ-Produced CO from Interfacial Catalytic Reactions. Nano Letters, 2016, 16, 7999-8004.	9.1	103
54	Designing superior solid electrolyte interfaces on silicon anodes for high-performance lithium-ion batteries. Nanoscale, 2019, 11, 19086-19104.	5.6	103

#	Article	IF	CITATIONS
55	Single crystalline CdS nanorods fabricated by a novel hydrothermal method. Chemical Physics Letters, 2003, 377, 654-657.	2.6	102
56	Carbon Nanocapsules as Nanoreactors for Controllable Synthesis of Encapsulated Iron and Iron Oxides: Magnetic Properties and Reversible Lithium Storage. Journal of Physical Chemistry C, 2011, 115, 3612-3620.	3.1	101
57	Cu–Ge core–shell nanowire arrays as three-dimensional electrodes for high-rate capability lithium-ion batteries. Journal of Materials Chemistry, 2012, 22, 1511-1515.	6.7	101
58	Efficient and highly light stable planar perovskite solar cells with graphene quantum dots doped PCBM electron transport layer. Nano Energy, 2017, 40, 345-351.	16.0	101
59	Shape-Control Fabrication and Characterization of the Airplane-like FeO(OH) and Fe2O3 Nanostructures. Crystal Growth and Design, 2006, 6, 351-353.	3.0	100
60	Selenium Nanotubes Synthesized by a Novel Solution Phase Approach. Journal of Physical Chemistry B, 2004, 108, 1179-1182.	2.6	98
61	Facile Synthesis of Fiveâ€fold Twinned, Starfishâ€like Rhodium Nanocrystals by Eliminating Oxidative Etching with a Chlorideâ€Free Precursor. Angewandte Chemie - International Edition, 2010, 49, 5296-5300.	13.8	97
62	Synthesis of NiO nanowires by a sol-gel process. Materials Letters, 2005, 59, 1967-1970.	2.6	95
63	Long Bi2S3nanowires prepared by a simple hydrothermal method. Nanotechnology, 2003, 14, 974-977.	2.6	94
64	Zero-power optoelectronic synaptic devices. Nano Energy, 2020, 73, 104790.	16.0	94
65	Interface engineering for efficient and stable chemical-doping-free graphene-on-silicon solar cells by introducing a graphene oxide interlayer. Journal of Materials Chemistry A, 2014, 2, 16877-16883.	10.3	93
66	Grown-in defects in nitrogen-doped Czochralski silicon. Journal of Applied Physics, 2002, 92, 188-194.	2.5	88
67	Nanoscale kinetics of asymmetrical corrosion in core-shell nanoparticles. Nature Communications, 2018, 9, 1011.	12.8	87
68	Lattice-Mismatch-Induced Twinning for Seeded Growth of Anisotropic Nanostructures. ACS Nano, 2015, 9, 3307-3313.	14.6	86
69	Ink Engineering of Inkjet Printing Perovskite. ACS Applied Materials & Interfaces, 2020, 12, 39082-39091.	8.0	85
70	Recombination activity of Σ3 boundaries in boron-doped multicrystalline silicon: Influence of iron contamination. Journal of Applied Physics, 2005, 97, 033701.	2.5	84
71	Preparation and characterization of water-soluble CdS nanocrystals by surface modification of ethylene diamine. Materials Letters, 2005, 59, 1024-1027.	2.6	83
72	Optimum Quantum Yield of the Light Emission from 2 to 10 nm Hydrosilylated Silicon Quantum Dots. Particle and Particle Systems Characterization, 2016, 33, 44-52.	2.3	83

#	Article	IF	CITATIONS
73	Size-controlled synthesis of Pd nanosheets for tunable plasmonic properties. CrystEngComm, 2015, 17, 1833-1838.	2.6	81
74	Direct CVD Growth of Graphene on Technologically Important Dielectric and Semiconducting Substrates. Advanced Science, 2018, 5, 1800050.	11.2	81
75	Electroluminescent synaptic devices with logic functions. Nano Energy, 2018, 54, 383-389.	16.0	80
76	Texturization of monocrystalline silicon with tribasic sodium phosphate. Solar Energy Materials and Solar Cells, 2003, 77, 255-263.	6.2	79
77	Fairly pure ultraviolet electroluminescence from ZnO-based light-emitting devices. Applied Physics Letters, 2006, 89, 111112.	3.3	79
78	Metal Oxide and Sulfide Hollow Spheres: Layer-By-Layer Synthesis and Their Application in Lithium-Ion Battery. Journal of Physical Chemistry B, 2008, 112, 14836-14842.	2.6	78
79	Effect of nitrogen–oxygen complex on electrical properties of Czochralski silicon. Applied Physics Letters, 1996, 68, 487-489.	3.3	77
80	Effects of complexing agent on CdS thin films prepared by chemical bath deposition. Materials Letters, 2004, 58, 5-9.	2.6	77
81	Fabrication of Flower-Like Silver Structures through Anisotropic Growth. Langmuir, 2011, 27, 6211-6217.	3.5	77
82	Investigation of texturization for monocrystalline silicon solar cells with different kinds of alkaline. Renewable Energy, 2004, 29, 2101-2107.	8.9	76
83	Directional CdS nanowires fabricated by chemical bath deposition. Journal of Crystal Growth, 2002, 246, 108-112.	1.5	75
84	Order-aligned Mn3O4 nanostructures as super high-rate electrodes for rechargeable lithium-ion batteries. Journal of Power Sources, 2013, 222, 32-37.	7.8	75
85	Trap Assisted Bulk Silicon Photodetector with High Photoconductive Gain, Low Noise, and Fast Response by Ag Hyperdoping. Advanced Optical Materials, 2018, 6, 1700638.	7.3	75
86	Three-dimensionally porous Fe3O4 as high-performance anode materials for lithium–ion batteries. Journal of Power Sources, 2014, 246, 198-203.	7.8	74
87	Improved performance and air stability of planar perovskite solar cells via interfacial engineering using a fullerene amine interlayer. Nano Energy, 2016, 28, 330-337.	16.0	74
88	Silicon nanocrystals: unfading silicon materials for optoelectronics. Materials Science and Engineering Reports, 2019, 138, 85-117.	31.8	74
89	From ZnO nanorods to 3D hollow microhemispheres: solvothermal synthesis, photoluminescence and gas sensor properties. Nanotechnology, 2007, 18, 455604.	2.6	73
90	Interface coupling in graphene/fluorographene heterostructure for high-performance graphene/silicon solar cells. Nano Energy, 2016, 28, 12-18.	16.0	73

#	Article	IF	CITATIONS
91	Scalable Synthesis of Pore-Rich Si/C@C Core–Shell-Structured Microspheres for Practical Long-Life Lithium-Ion Battery Anodes. ACS Applied Materials & Interfaces, 2022, 14, 10308-10318.	8.0	73
92	Straight and Thin ZnO Nanorods:Â Hectogram-Scale Synthesis at Low Temperature and Cathodoluminescence. Journal of Physical Chemistry B, 2006, 110, 827-830.	2.6	72
93	Homogeneous coating of Au and SnO2 nanocrystals on carbon nanotubes via layer-by-layer assembly: a new ternary hybrid for a room-temperature CO gas sensor. Chemical Communications, 2008, , 6182.	4.1	72
94	Room temperature electrically pumped ultraviolet random lasing from ZnO nanorod arrays on Si. Optics Express, 2009, 17, 14426.	3.4	71
95	Low-cost solar grade silicon purification process with Al–Si system using a powder metallurgy technique. Separation and Purification Technology, 2011, 77, 33-39.	7.9	70
96	Facile synthesis of Pd–Pt alloy concave nanocubes with high-index facets as electrocatalysts for methanol oxidation. CrystEngComm, 2014, 16, 2411-2416.	2.6	69
97	Elimination of Interfacialâ€Electrochemicalâ€Reactionâ€Induced Polarization in Perovskite Single Crystals for Ultrasensitive and Stable Xâ€Ray Detector Arrays. Advanced Materials, 2021, 33, e2103078.	21.0	69
98	Boron- and Phosphorus-Hyperdoped Silicon Nanocrystals. Particle and Particle Systems Characterization, 2015, 32, 213-221.	2.3	68
99	Light-Emitting Diodes Based on Colloidal Silicon Quantum Dots with Octyl and Phenylpropyl Ligands. ACS Applied Materials & Interfaces, 2018, 10, 5959-5966.	8.0	68
100	Dualâ€Modal Optoelectronic Synaptic Devices with Versatile Synaptic Plasticity. Advanced Functional Materials, 2022, 32, 2107973.	14.9	68
101	Synthesis of Co2SnO4@C core–shell nanostructures with reversible lithium storage. Journal of Power Sources, 2011, 196, 10234-10239.	7.8	66
102	One-pot, large-scale synthesis of SnO2 nanotubes at room temperature. Chemical Communications, 2008, , 3028.	4.1	65
103	Synthesis of polycrystalline SnO2 nanotubes on carbon nanotube template for anode material of lithium-ion battery. Materials Research Bulletin, 2009, 44, 211-215.	5.2	64
104	An 8.68% Efficiency Chemically-Doped-Free Graphene–Silicon Solar Cell Using Silver Nanowires Network Buried Contacts. ACS Applied Materials & Interfaces, 2015, 7, 4135-4141.	8.0	64
105	Large-scale synthesis of Si@C three-dimensional porous structures as high-performance anode materials for lithium-ion batteries. Journal of Materials Chemistry A, 2014, 2, 20494-20499.	10.3	63
106	Sizeâ€Dependent Structures and Optical Absorption of Boronâ€Hyperdoped Silicon Nanocrystals. Advanced Optical Materials, 2016, 4, 700-707.	7.3	63
107	Synthesis of ultrafine lanthanum hydroxide nanorods by a simple hydrothermal process. Materials Letters, 2004, 58, 1180-1182.	2.6	62
108	Hydrothermal synthesis, characterization and properties of SnS nanoflowers. Materials Letters, 2006, 60, 2686-2689.	2.6	62

#	Article	IF	CITATIONS
109	Silicene oxides: formation, structures and electronic properties. Scientific Reports, 2013, 3, 3507.	3.3	62
110	Ultrathin Two-Dimensional Pd-Based Nanorings as Catalysts for Hydrogenation with High Activity and Stability. Small, 2015, 11, 4745-4752.	10.0	62
111	Enhanced performance and light soaking stability of planar perovskite solar cells using an amine-based fullerene interfacial modifier. Journal of Materials Chemistry A, 2016, 4, 18509-18515.	10.3	62
112	Perovskite Bifunctional Device with Improved Electroluminescent and Photovoltaic Performance through Interfacial Energyâ€Band Engineering. Advanced Materials, 2019, 31, e1902543.	21.0	62
113	Selfâ€Powered FA <sub>0.55</sub> MA <sub>0.45</sub> PbI <sub>3</sub> Singleâ€Crystal Perovskite Xâ€Ray Detectors with High Sensitivity. Advanced Functional Materials, 2022, 32, 2109149.	14.9	62
114	Hydrothermal growth and characterization of magnetite (Fe3O4) thin films. Surface and Coatings Technology, 2007, 201, 5870-5874.	4.8	61
115	Phase-Selective Synthesis and Self-Assembly of Monodisperse Copper Sulfide Nanocrystals. Journal of Physical Chemistry C, 2008, 112, 13390-13394.	3.1	61
116	Novel CuS hollow spheres fabricated by a novel hydrothermal method. Microporous and Mesoporous Materials, 2005, 80, 153-156.	4.4	60
117	Hydrothermal synthesis of flower-like SrCO3 nanostructures. Materials Letters, 2005, 59, 420-422.	2.6	60
118	ZnO:Eu thin-films: Sol–gel derivation and strong photoluminescence from 5D0→7F0 transition of Eu3+ ions. Journal of Alloys and Compounds, 2007, 431, 317-320.	5.5	60
119	Layer-stacked tin disulfide nanorods in silica nanoreactors with improved lithium storage capabilities. Nanoscale, 2012, 4, 4002.	5.6	60
120	Atomistic Surface Passivation of CH <sub>3</sub> NH <sub>3</sub> Pbl <sub>3</sub> Perovskite Single Crystals for Highly Sensitive Coplanar-Structure X-Ray Detectors. Research, 2020, 2020, 5958243.	5.7	60
121	InOOH Hollow Spheres Synthesized by a Simple Hydrothermal Reaction. Journal of Physical Chemistry B, 2005, 109, 20676-20679.	2.6	59
122	Large-scale synthesis and application of SnS2–graphene nanocomposites as anode materials for lithium-ion batteries with enhanced cyclic performance and reversible capacity. Journal of Alloys and Compounds, 2013, 580, 457-464.	5.5	59
123	Rational design of three-dimensional macroporous silicon as high performance Li-ion battery anodes with long cycle life. Journal of Power Sources, 2016, 331, 76-81.	7.8	59
124	An improved seed-mediated growth method to coat complete silver shells onto silica spheres for surface-enhanced Raman scattering. Colloids and Surfaces A: Physicochemical and Engineering Aspects, 2011, 387, 17-22.	4.7	58
125	Impact of solar irradiance intensity and temperature on the performance of compensated crystalline silicon solar cells. Solar Energy Materials and Solar Cells, 2014, 128, 427-434.	6.2	58
126	High Efficiency Organic/Silicon-Nanowire Hybrid Solar Cells: Significance of Strong Inversion Layer. Scientific Reports, 2015, 5, 17371.	3.3	58

#	Article	IF	CITATIONS
127	Electronic and magnetic properties of graphene, silicene and germanene with varying vacancy concentration. AIP Advances, 2017, 7, .	1.3	58
128	Synthesis and Field Emission Characteristics of Bilayered ZnO Nanorod Array Prepared by Chemical Reaction. Journal of Physical Chemistry B, 2005, 109, 17055-17059.	2.6	57
129	Effect of pressure on nanocrystalline diamond films deposition by hot filament CVD technique from CH4/H2 gas mixture. Surface and Coatings Technology, 2007, 202, 261-267.	4.8	57
130	Effect of oxygen precipitation on the performance of Czochralski silicon solar cells. Solar Energy Materials and Solar Cells, 2011, 95, 3148-3151.	6.2	57
131	Low-Temperature Growth of Uniform ZnO Particles with Controllable Ellipsoidal Morphologies and Characteristic Luminescence Patterns. Journal of Physical Chemistry B, 2006, 110, 19147-19153.	2.6	56
132	Carbon nanotube-based magnetic-fluorescent nanohybrids as highly efficient contrast agents for multimodal cellular imaging. Journal of Materials Chemistry, 2010, 20, 9895.	6.7	56
133	Facile synthesis of uniform MWCNT@Si nanocomposites as high-performance anode materials for lithium-ion batteries. Journal of Alloys and Compounds, 2015, 622, 966-972.	5.5	56
134	Temperature-Dependent Raman Scattering of Silicon Nanowires. Journal of Physical Chemistry B, 2006, 110, 1229-1234.	2.6	55
135	Electroluminescence of SnO2â^•p-Si heterojunction. Applied Physics Letters, 2008, 92, .	3.3	55
136	First-Principles Study of 2.2 nm Silicon Nanocrystals Doped with Boron. Journal of Physical Chemistry C, 2011, 115, 9838-9843.	3.1	55
137	Rareâ€Earth Doped ZnO Films: A Material Platform to Realize Multicolor and Nearâ€Infrared Electroluminescence. Advanced Optical Materials, 2014, 2, 240-244.	7.3	55
138	Facile synthesis of Rh–Pd alloy nanodendrites as highly active and durable electrocatalysts for oxygen reduction reaction. Nanoscale, 2014, 6, 7012-7018.	5.6	55
139	Cu–Sn Core–Shell Nanowire Arrays as Three-Dimensional Electrodes for Lithium-Ion Batteries. Journal of Physical Chemistry C, 2011, 115, 23620-23624.	3.1	54
140	Silver Nanoshell Plasmonically Controlled Emission of Semiconductor Quantum Dots in the Strong Coupling Regime. ACS Nano, 2016, 10, 4154-4163.	14.6	54
141	Synthesis of CdS nanotubes by chemical bath deposition. Journal of Crystal Growth, 2004, 263, 372-376.	1.5	53
142	Origin of room temperature ferromagnetism in MgO films. Applied Physics Letters, 2013, 102, .	3.3	53
143	Impurity engineering of Czochralski silicon. Materials Science and Engineering Reports, 2013, 74, 1-33.	31.8	52
144	Stabilizing Fullerene for Burnâ€inâ€Free and Stable Perovskite Solar Cells under Ultraviolet Preconditioning and Light Soaking. Advanced Materials, 2021, 33, e2006910.	21.0	52

#	Article	IF	CITATIONS
145	Bioinspired molecules design for bilateral synergistic passivation in buried interfaces of planar perovskite solar cells. Nano Research, 2022, 15, 1069-1078.	10.4	52
146	First-Principles Study on the Surface Chemistry of 1.4 nm Silicon Nanocrystals: Case of Hydrosilylation. Journal of Physical Chemistry C, 2012, 116, 19434-19443.	3.1	51
147	Critical Role of Dopant Location for P-Doped Si Nanocrystals. Journal of Physical Chemistry C, 2011, 115, 661-666.	3.1	50
148	Nitrogen effects on thermal donor and shallow thermal donor in silicon. Journal of Applied Physics, 1995, 77, 943-944.	2.5	49
149	Structure and luminescence evolution of annealed Europium-doped silicon oxides films. Optics Express, 2010, 18, 27191.	3.4	49
150	CoO/NiSix core–shell nanowire arrays as lithium-ion anodes with high rate capabilities. Nanoscale, 2012, 4, 991-996.	5.6	49
151	Synthesis of cadmium hydroxide nanoflake and nanowisker by hydrothermal method. Materials Letters, 2005, 59, 56-58.	2.6	48
152	Controllable growth of dendrite-like CuO nanostructures by ethylene glycol assisted hydrothermal process. Materials Research Bulletin, 2008, 43, 1291-1296.	5.2	48
153	Cu–Si1â^'xGex core–shell nanowire arrays as three-dimensional electrodes for high-rate capability lithium-ion batteries. Journal of Power Sources, 2012, 208, 434-439.	7.8	48
154	Tuning Surface Structure of Pd <sub>3</sub> Pb/Pt <i><sub>n</sub></i> Pb Nanocrystals for Boosting the Methanol Oxidation Reaction. Advanced Science, 2019, 6, 1902249.	11.2	48
155	Strain-Induced Corrosion Kinetics at Nanoscale Are Revealed in Liquid: Enabling Control of Corrosion Dynamics of Electrocatalysis. CheM, 2020, 6, 2257-2271.	11.7	48
156	An MOFâ€Based Luminescent Sensor Array for Pattern Recognition and Quantification of Metal Ions. Advanced Optical Materials, 2021, 9, 2002180.	7.3	48
157	Self-assembly of CdS: from nanoparticles to nanorods and arrayed nanorod bundles. Materials Chemistry and Physics, 2005, 93, 65-69.	4.0	47
158	Effect of the substrate temperature on the crystallization of TiO2 films prepared by DC reactive magnetron sputtering. Journal of Crystal Growth, 2007, 300, 551-554.	1.5	47
159	Selfâ€Organized Fullerene Interfacial Layer for Efficient and Lowâ€Temperature Processed Planar Perovskite Solar Cells with High UVâ€Light Stability. Advanced Science, 2017, 4, 1700018.	11.2	47
160	Synthesis of La1â^xCaxMnO3 nanowires by a sol–gel process. Chemical Physics Letters, 2002, 363, 579-582.	2.6	46
161	MgO nanostructures synthesized by thermal evaporation. Materials Science and Engineering C, 2006, 26, 1097-1101.	7.3	46
162	Germanium effect on void defects in Czochralski silicon. Journal of Crystal Growth, 2002, 243, 371-374.	1.5	45

#	Article	IF	CITATIONS
163	In situ study of the growth of two-dimensional palladium dendritic nanostructures using liquid-cell electron microscopy. Chemical Communications, 2014, 50, 9447.	4.1	45
164	High efficiency organic/silicon hybrid solar cells with doping-free selective emitter structure induced by a WO3 thin interlayer. Nano Energy, 2015, 16, 54-61.	16.0	45
165	Higher quality mono-like cast silicon with induced grain boundaries. Solar Energy Materials and Solar Cells, 2015, 140, 121-125.	6.2	45
166	Improvement of conversion efficiency of multicrystalline silicon solar cells by incorporating reactive ion etching texturing. Solar Energy Materials and Solar Cells, 2014, 127, 21-26.	6.2	43
167	A high-quality round-shaped monolayer MoS <sub>2</sub> domain and its transformation. Nanoscale, 2016, 8, 219-225.	5.6	43
168	Strain-induced Stranski–Krastanov growth of Pd@Pt core–shell hexapods and octapods as electrocatalysts for methanol oxidation. Nanoscale, 2017, 9, 11077-11084.	5.6	43
169	An Interlayer with Strong Pb-Cl Bond Delivers Ultraviolet-Filter-Free, Efficient, and Photostable Perovskite Solar Cells. IScience, 2019, 21, 217-227.	4.1	43
170	Simple Near-Infrared Electron Acceptors for Efficient Photovoltaics and Sensitive Photodetectors. ACS Applied Materials & Interfaces, 2020, 12, 39515-39523.	8.0	43
171	Single-crystalline SnS2nano-belts fabricated by a novel hydrothermal method. Journal of Physics Condensed Matter, 2003, 15, L661-L665.	1.8	42
172	Synthesis of MgO nanotube bundles. Nanotechnology, 2004, 15, 1004-1008.	2.6	42
173	One-Pot Synthesis of Biocompatible CdSe/CdS Quantum Dots and Their Applications as Fluorescent Biological Labels. Nanoscale Research Letters, 2011, 6, 31.	5.7	42
174	Optical properties of sputtered hexagonal CdZnO films with band gap energies from 1.8 to 3.3eV. Journal of Alloys and Compounds, 2011, 509, 6599-6602.	5.5	42
175	A critical SiO <sub>x</sub> layer on Si porous structures to construct highly-reversible anode materials for lithium-ion batteries. Chemical Communications, 2017, 53, 6101-6104.	4.1	42
176	Size-dependent magnetic properties of branchlike nickel oxide nanocrystals. AIP Advances, 2017, 7, .	1.3	42
177	High and Fast Response of a Graphene–Silicon Photodetector Coupled with 2D Fractal Platinum Nanoparticles. Advanced Optical Materials, 2018, 6, 1700793.	7.3	42
178	Assembling CoSn3 nanoparticles on multiwalled carbon nanotubes with enhanced lithium storage properties. Nanoscale, 2011, 3, 1798.	5.6	41
179	Theoretical Study of Chlorine for Silicon Nanocrystals. Journal of Physical Chemistry C, 2011, 115, 12822-12825.	3.1	41
180	Layer-by-layer synthesis of γ-Fe2O3@SnO2@C porous core–shell nanorods with high reversible capacity in lithium-ion batteries. Nanoscale, 2013, 5, 4744.	5.6	41

#	Article	IF	CITATIONS
181	Low-voltage driven â^¼1.54 <i>μ</i> m electroluminescence from erbium-doped ZnO/ <i>p</i> +-Si heterostructured devices: Energy transfer from ZnO host to erbium ions. Applied Physics Letters, 2013, 102, .	3.3	41
182	The enhanced efficiency of graphene–silicon solar cells by electric field doping. Nanoscale, 2015, 7, 7072-7077.	5.6	41
183	Bonding of Oxygen at the Oxide/Nanocrystal Interface of Oxidized Silicon Nanocrystals: An <i>Ab Initio</i> Study. Journal of Physical Chemistry C, 2010, 114, 8774-8781.	3.1	40
184	Fluorine-Passivated Silicon Nanocrystals: Surface Chemistry versus Quantum Confinement. Journal of Physical Chemistry C, 2012, 116, 5401-5406.	3.1	40
185	Carbon dioxide as a green carbon source for the synthesis of carbon cages encapsulating porous silicon as high performance lithium-ion battery anodes. Nanoscale, 2018, 10, 5626-5633.	5.6	40
186	Effects of nitrogen on dislocations in silicon during heat treatment. Physica B: Condensed Matter, 1999, 273-274, 553-556.	2.7	39
187	Array-orderly single crystalline silicon nano-wires. Chemical Physics Letters, 2003, 367, 528-532.	2.6	39
188	Silicon nanowires fabricated by thermal evaporation of silicon monoxide. Physica E: Low-Dimensional Systems and Nanostructures, 2004, 23, 131-134.	2.7	39
189	Electron-beam-induced current study of hydrogen passivation on grain boundaries in multicrystalline silicon: Influence of GB character and impurity contamination. Physica B: Condensed Matter, 2005, 364, 162-169.	2.7	39
190	Synthesis of aluminium borate nanowires by sol–gel method. Materials Research Bulletin, 2005, 40, 1551-1557.	5.2	39
191	Low-temperature chemical solution route for ZnO based sulfide coaxial nanocables: general synthesis and gas sensor application. Nanotechnology, 2007, 18, 115619.	2.6	39
192	Vertically ordered Ni3Si2/Si nanorod arrays as anode materials for high-performance Li-ion batteries. Nanoscale, 2012, 4, 5343.	5.6	39
193	Carbon Nanotube-ZnO Nanosphere Heterostructures: Low-Temperature Chemical Reaction Synthesis, Photoluminescence, and Their Application for Room Temperature NH <sub>3</sub> Gas Sensor. Science of Advanced Materials, 2009, 1, 13-17.	0.7	39
194	Visible-blind short-wavelength infrared photodetector with high responsivity based on hyperdoped silicon. Photonics Research, 2019, 7, 351.	7.0	39
195	Oxygen precipitation in nitrogen-doped Czochralski silicon. Physica B: Condensed Matter, 1999, 273-274, 308-311.	2.7	38
196	Sequential occurrence of ZnO nanopaticles, nanorods, and nanotips during hydrothermal process in a dilute aqueous solution. Materials Letters, 2005, 59, 3393-3397.	2.6	38
197	Graphene coupled with Pt cubic nanoparticles for high performance, air-stable graphene-silicon solar cells. Nano Energy, 2017, 32, 225-231.	16.0	38
198	An inverted planar solar cell with 13% efficiency and a sensitive visible light detector based on orientation regulated 2D perovskites. Journal of Materials Chemistry A, 2018, 6, 24633-24640.	10.3	38

#	ARTICLE	IF	CITATIONS
199	Hydrothermal synthesis of flower-like Bi2S3with nanorods in the diameter region of 30 nm. Nanotechnology, 2004, 15, 1122-1125.	2.6	37
200	Layer-by-layer assembly synthesis of ZnO/SnO2 composite nanowire arrays as high-performance anode for lithium-ion batteries. Materials Research Bulletin, 2011, 46, 2378-2384.	5.2	37
201	Synthesis of Co3O4@SnO2@C core-shell nanorods with superior reversible lithium-ion storage. RSC Advances, 2012, 2, 9511.	3.6	37
202	Silicon-nanocrystal-incorporated ternary hybrid solar cells. Nano Energy, 2016, 26, 305-312.	16.0	37
203	Facile synthesis of Ru-decorated Pt cubes and icosahedra as highly active electrocatalysts for methanol oxidation. Nanoscale, 2016, 8, 12812-12818.	5.6	37
204	Local epitaxial growth of Au-Rh core-shell star-shaped decahedra: A case for studying electronic and ensemble effects in hydrogen evolution reaction. Applied Catalysis B: Environmental, 2020, 263, 118255.	20.2	37
205	General Solution Route for Nanoplates of Hexagonal Oxide or Hydroxide. Journal of Physical Chemistry B, 2006, 110, 11196-11198.	2.6	36
206	Ni3Si2–Si nanowires on Ni foam as a high-performance anode of Li-ion batteries. Electrochemistry Communications, 2011, 13, 1443-1446.	4.7	36
207	Effect of tin on point defects and oxygen precipitation in Czochralski silicon: Experimental and theoretical studies. Journal of Applied Physics, 2013, 113, .	2.5	36
208	13.7% Efficiency graphene–gallium arsenide Schottky junction solar cells with a P3HT hole transport layer. Nano Energy, 2015, 16, 91-98.	16.0	36
209	Seed-mediated growth of Au nanorings with size control on Pd ultrathin nanosheets and their tunable surface plasmonic properties. Nanoscale, 2016, 8, 3704-3710.	5.6	36
210	Mitigating Ion Migration by Polyethylene Glycol-Modified Fullerene for Perovskite Solar Cells with Enhanced Stability. ACS Energy Letters, 2021, 6, 3864-3872.	17.4	36
211	Star-shaped PbS crystals fabricated by a novel hydrothermal method. Journal of Physics Condensed Matter, 2003, 15, 7611-7615.	1.8	35
212	Sonochemical synthesis of amorphous long silver sulfide nanowires. Materials Letters, 2007, 61, 235-238.	2.6	35
213	A facile two-step hydrothermal route for the synthesis of γ-Fe2O3 nanocrystals and their magnetic properties. Journal of Materials Science, 2007, 42, 9205-9209.	3.7	35
214	General Layer-By-Layer Approach To Composite Nanotubes and Their Enhanced Lithium-Storage and Gas-Sensing Properties. Chemistry of Materials, 2009, 21, 5264-5271.	6.7	35
215	Tunable surface plasmon resonance frequencies of monodisperse indium tin oxide nanoparticles by controlling composition, size, and morphology. Nanoscale Research Letters, 2014, 9, 547.	5.7	35
216	Doping Si nanocrystals embedded in SiO <mml:math xmlns:mml="http://www.w3.org/1998/Math/MathML"&gt;<mml:msub><mml:mrow /&gt;<mml:mn>2</mml:mn></mml:mrow </mml:msub>with P in the framework of density functional theory. Physical Review B, 2014, 89, .</mml:math 	3.2	35

#	Article	IF	CITATIONS
217	Multicolor and near-infrared electroluminescence from the light-emitting devices with rare-earth doped TiO2 films. Applied Physics Letters, 2015, 107, .	3.3	35
218	A ternary organic electron transport layer for efficient and photostable perovskite solar cells under full spectrum illumination. Journal of Materials Chemistry A, 2018, 6, 5566-5573.	10.3	35
219	CO <sub>2</sub> Footprint of Thermal Versus Photothermal CO <sub>2</sub> Catalysis. Small, 2021, 17, e2007025.	10.0	35
220	Enhancement effect of germanium on oxygen precipitation in Czochralski silicon. Journal of Applied Physics, 2006, 99, 073509.	2.5	34
221	Labeling transplanted mice islet with polyvinylpyrrolidone coated superparamagnetic iron oxide nanoparticles for <i>in vivo</i> detection by magnetic resonance imaging. Nanotechnology, 2009, 20, 365101.	2.6	34
222	The location and doping effect of boron in Si nanocrystals embedded silicon oxide film. Applied Physics Letters, 2013, 102, .	3.3	34
223	Texturization of cast multicrystalline silicon for solar cells. Semiconductor Science and Technology, 2004, 19, 485-489.	2.0	33
224	Germanium effect on oxygen precipitation in Czochralski silicon. Journal of Applied Physics, 2004, 96, 4161-4165.	2.5	33
225	Synthesis of flower-like CdS nanostructures by organic-free hydrothermal process and their optical properties. Materials Letters, 2007, 61, 3507-3510.	2.6	33
226	A Versatile Approach for the Synthesis of ZnO Nanorod-Based Hybrid Nanomaterials via Layer-by-Layer Assembly. Journal of Physical Chemistry C, 2009, 113, 8147-8151.	3.1	33
227	Synthesis of hexagonal structured wurtzite and chalcopyrite CuInS2 via a simple solution route. Nanoscale Research Letters, 2011, 6, 562.	5.7	33
228	Waterâ€Dispersible Siliconâ€Quantumâ€Dotâ€Containing Micelles Selfâ€Assembled from an Amphiphilic Polymer. Particle and Particle Systems Characterization, 2014, 31, 751-756.	2.3	33
229	Density functional theory study on boron- and phosphorus-doped hydrogen-passivated silicene. Physical Chemistry Chemical Physics, 2015, 17, 4146-4151.	2.8	33
230	Multimetallic AuPd@Pd@Pt core-interlayer-shell icosahedral electrocatalysts for highly efficient oxygen reduction reaction. Science Bulletin, 2018, 63, 494-501.	9.0	33
231	Wetting behaviors and applications of metal-catalyzed CVD grown graphene. Journal of Materials Chemistry A, 2018, 6, 22437-22464.	10.3	33
232	Tailoring the Edge Sites of 2D Pd Nanostructures with Different Fractal Dimensions for Enhanced Electrocatalytic Performance. Advanced Science, 2018, 5, 1800430.	11.2	33
233	Formation of pnp bipolar structure by thermal donors in nitrogen-containing p-type Czochralski silicon wafers. Applied Physics Letters, 2002, 81, 496-498.	3.3	32
234	Large-scale synthesis of Ag–Si core–shell nanowall arrays as high-performance anode materials of Li-ion batteries. Journal of Materials Chemistry A, 2014, 2, 13949-13954.	10.3	32

#	Article	IF	CITATIONS
235	Performance Improvement of Graphene/Silicon Photodetectors Using High Work Function Metal Nanoparticles with Plasma Effect. Advanced Optical Materials, 2018, 6, 1701243.	7.3	32
236	CH <sub>3</sub> NH <sub>3</sub> PbBr <sub>3</sub> Quantum Dot-Induced Nucleation for High Performance Perovskite Light-Emitting Solar Cells. ACS Applied Materials & Interfaces, 2018, 10, 22320-22328.	8.0	32
237	The effect of germanium doping on oxygen donors in Czochralski-grown silicon. Journal of Physics Condensed Matter, 2004, 16, 5745-5750.	1.8	31
238	Cobalt ferrite nanorings: Ostwald ripening dictated synthesis and magnetic properties. Chemical Communications, 2008, , 5648.	4.1	31
239	Localized surface plasmon enhanced photoluminescence from ZnO films: Extraction direction and emitting layer thickness. Journal of Applied Physics, 2009, 106, 063120.	2.5	31
240	Shape and phase control of CdS nanocrystals using cationic surfactant in noninjection synthesis. Nanoscale Research Letters, 2011, 6, 374.	5.7	31
241	Low-voltage driven visible and infrared electroluminescence from light-emitting device based on Er-doped TiO2/ <i>p</i> +-Si heterostructure. Applied Physics Letters, 2012, 100, .	3.3	31
242	Kinetically-controlled growth of cubic and octahedral Rh–Pd alloy oxygen reduction electrocatalysts with high activity and durability. Nanoscale, 2015, 7, 301-307.	5.6	31
243	Porous silicon in carbon cages as high-performance lithium-ion battery anode Materials. Electrochimica Acta, 2017, 252, 438-445.	5.2	31
244	Developing near-infrared quantum-dot light-emitting diodes to mimic synaptic plasticity. Science China Materials, 2019, 62, 1470-1478.	6.3	31
245	Crystalline boron oxide nanowires on silicon substrate. Physica E: Low-Dimensional Systems and Nanostructures, 2005, 27, 319-324.	2.7	30
246	Controlling the growth and field emission properties of silicide nanowire arrays by direct silicification of Ni foil. Nanotechnology, 2008, 19, 375602.	2.6	30
247	Freestanding doped silicon nanocrystals synthesized by plasma. Journal Physics D: Applied Physics, 2015, 48, 314006.	2.8	30
248	Raman spectrum of array-ordered crystalline silicon nanowires. Physica E: Low-Dimensional Systems and Nanostructures, 2004, 23, 221-225.	2.7	29
249	Correlation between luminescence and structural evolution of Si-rich silicon oxide film annealed at different temperatures. Journal of Applied Physics, 2007, 101, 103504.	2.5	29
250	Influence of germanium doping on the mechanical strength of Czochralski silicon wafers. Journal of Applied Physics, 2008, 103, .	2.5	29
251	Single-crystalline Pd square nanoplates enclosed by {100} facets on reduced graphene oxide for formic acid electro-oxidation. Chemical Communications, 2016, 52, 14204-14207.	4.1	29
252	Solvation effect in precursor solution enables over 16% efficiency in thick 2D perovskite solar cells. Journal of Materials Chemistry A, 2019, 7, 19423-19429.	10.3	29

#	Article	IF	CITATIONS
253	Hydrothermal Synthesis and Characterization of Zirconia Nanocrystallites. Journal of the American Ceramic Society, 2007, 90, 1334-1338.	3.8	28
254	Preparation of echinus-like SiO2@Ag structures with the aid of the HCP phase. Chemical Communications, 2011, 47, 5169.	4.1	28
255	Formation of nanostructured emitter for silicon solar cells using catalytic silver nanoparticles. Applied Surface Science, 2013, 264, 621-624.	6.1	28
256	A model for distribution of oxygen in multicrystalline silicon ingot grown by directional solidification. Solar Energy Materials and Solar Cells, 2007, 91, 1688-1691.	6.2	27
257	Hydrothermal Synthesis and Photoluminescence Properties of La <sub>2â^'<i>x</i></sub> Eu <sub><i>x</i></sub> Sn <sub>2</sub> O <sub>7</sub> ( <i>x</i> =0–2.0) Nanocrystals. Journal of the American Ceramic Society, 2007, 90, 3095-3098.	3.8	27
258	Reflectivity of porous-pyramids structured silicon surface. Applied Surface Science, 2010, 257, 472-475.	6.1	27
259	Nanostructured hybrid cobalt oxide/copper electrodes of lithium-ion batteries with reversible high-rate capabilities. Journal of Alloys and Compounds, 2012, 521, 83-89.	5.5	27
260	Field emission performance enhancement of Au nanoparticles doped graphene emitters. Applied Physics Letters, 2013, 103, .	3.3	27
261	Voltage-controlled synthesis of Cu–Li <sub>2</sub> O@Si core–shell nanorod arrays as high-performance anodes for lithium-ion batteries. Journal of Materials Chemistry A, 2014, 2, 20510-20514.	10.3	27
262	Multicrystalline silicon crystal assisted by silicon flakes as seeds. Solar Energy Materials and Solar Cells, 2018, 174, 202-205.	6.2	27
263	Ultra-small Rh nanoparticles supported on WO <sub>3â^'x</sub> nanowires as efficient catalysts for visible-light-enhanced hydrogen evolution from ammonia borane. Nanoscale Advances, 2019, 1, 3941-3947.	4.6	27
264	Donor formation in nitrogen doped silicon. Journal of Applied Physics, 1996, 80, 1493-1498.	2.5	26
265	Intrinsic gettering in germanium-doped Czochralski crystal silicon crystals. Journal of Crystal Growth, 2003, 250, 359-363.	1.5	26
266	Formation of a denuded zone in nitrogen-doped Czochralski silicon wafer treated by ramping anneals. Semiconductor Science and Technology, 2005, 20, 228-232.	2.0	26
267	Low temperature chemical reaction synthesis of single-crystalline Eu(OH)3nanorods and their thermal conversion to Eu2O3nanorods. Nanotechnology, 2007, 18, 065605.	2.6	26
268	Large-scale synthesis of silicon arrays of nanowire on titanium substrate as high-performance anode of Li-ion batteries. Journal of Alloys and Compounds, 2012, 526, 53-58.	5.5	26
269	Surface modification of chlorine-passivated silicon nanocrystals. Physical Chemistry Chemical Physics, 2013, 15, 1815.	2.8	26
270	PdCu alloy nanodendrites with tunable composition as highly active electrocatalysts for methanol oxidation. RSC Advances, 2017, 7, 5800-5806.	3.6	26

#	Article	IF	CITATIONS
271	Vacuum co-deposited CH3NH3PbI3 films by controlling vapor pressure for efficient planar perovskite solar cells. Solar Energy, 2019, 181, 339-344.	6.1	26
272	Narrowband Nearâ€Infrared Photodetector Enabled by Dual Functional Internalâ€Filterâ€Induced Selective Charge Collection. Advanced Optical Materials, 2021, 9, 2100288.	7.3	26
273	A versatile solution route for oxide/sulfide core–shell nanostructures and nonlayered sulfide nanotubes. Nanotechnology, 2005, 16, 2721-2725.	2.6	25
274	Carbon-assisted synthesis of aligned ZnO nanowires. Materials Letters, 2005, 59, 2710-2714.	2.6	25
275	Photoluminescence of Tb3+ doped SiNx films grown by plasma-enhanced chemical vapor deposition. Journal of Applied Physics, 2006, 100, 083106.	2.5	25
276	Suppression of boron–oxygen defects in p-type Czochralski silicon by germanium doping. Applied Physics Letters, 2010, 97, 051903.	3.3	25
277	Ambient Engineering for High-Performance Organic–Inorganic Perovskite Hybrid Solar Cells. ACS Applied Materials & Interfaces, 2016, 8, 21505-21511.	8.0	25
278	Amine treatment induced perovskite nanowire network in perovskite solar cells: efficient surface passivation and carrier transport. Nanotechnology, 2018, 29, 065401.	2.6	25
279	Seedâ€Assisted Growth of Castâ€Mono Silicon for Photovoltaic Application: Challenges and Strategies. Solar Rrl, 2020, 4, 1900486.	5.8	25
280	Sn-Doped Bi <sub>2</sub> O <sub>3</sub> nanosheets for highly efficient electrochemical CO <sub>2</sub> reduction toward formate production. Nanoscale, 2021, 13, 19610-19616.	5.6	25
281	Stable Cu Catalysts Supported by Twoâ€dimensional SiO <sub>2</sub> with Strong Metal–Support Interaction. Advanced Science, 2022, 9, e2104972.	11.2	25
282	Photoluminescence of oxidized porous silicon under UV-light illumination. Materials Science and Engineering B: Solid-State Materials for Advanced Technology, 2005, 116, 95-98.	3.5	24
283	Thermal-desorption induced enhancement and patterning of ultraviolet emission in chemically grown ZnO. Nanotechnology, 2006, 17, 2789-2793.	2.6	24
284	Electrophotoluminescence of ZnO film. Applied Physics Letters, 2007, 91, 021105.	3.3	24
285	Influence of substrates in ZnO devices on the surface plasmon enhanced light emission. Optics Express, 2008, 16, 8896.	3.4	24
286	Functionalization of carbon nanotubes with magnetic nanoparticles: general nonaqueous synthesis and magnetic properties. Nanotechnology, 2008, 19, 315604.	2.6	24
287	A General Approach for Uniform Coating of a Metal Layer on MWCNTs via Layer-by-Layer Assembly. Journal of Physical Chemistry C, 2009, 113, 17387-17391.	3.1	24
288	Germanium-doped Czochralski silicon for photovoltaic applications. Solar Energy Materials and Solar Cells, 2011, 95, 2466-2470.	6.2	24

#	Article	IF	CITATIONS
289	Enhancement of light-extraction efficiency of SiNx light emitting devices through a rough Ag island film. Applied Physics Letters, 2012, 100, 031113.	3.3	24
290	Enhanced solar energy conversion in Au-doped, single-wall carbon nanotube-Si heterojunction cells. Nanoscale Research Letters, 2013, 8, 225.	5.7	24
291	SiGe porous nanorod arrays as high-performance anode materials for lithium-ion batteries. Journal of Alloys and Compounds, 2013, 577, 564-568.	5.5	24
292	Morphology and composition controlled synthesis of flower-like silver nanostructures. Nanoscale Research Letters, 2014, 9, 302.	5.7	24
293	Fulleropyrrolidinium Iodide As an Efficient Electron Transport Layer for Air-Stable Planar Perovskite Solar Cells. ACS Applied Materials & Interfaces, 2016, 8, 34612-34619.	8.0	24
294	Silicon-Quantum-Dot Light-Emitting Diodes With Interlayer-Enhanced Hole Transport. IEEE Photonics Journal, 2017, 9, 1-10.	2.0	24
295	Crystallization and disappearance of defects of the annealed silicon nanowires. Microelectronic Engineering, 2003, 66, 65-69.	2.4	23
296	Effect of intrinsic point defects on copper precipitation in large-diameter Czochralski silicon. Applied Physics Letters, 2003, 83, 3048-3050.	3.3	23
297	Temperature dependence of the first-order Raman scattering in silicon nanowires. Scripta Materialia, 2006, 55, 183-186.	5.2	23
298	Hybrid nanostructures of Au nanocrystals and ZnO nanorods: Layer-by-layer assembly and tunable blue-shift band gap emission. Materials Research Bulletin, 2009, 44, 889-892.	5.2	23
299	Functionalization of ZnO nanorods with γ-Fe2O3 nanoparticles: Layer-by-layer synthesis, optical and magnetic properties. Materials Chemistry and Physics, 2010, 124, 908-911.	4.0	23
300	Preparation of metal@silica core–shell particle films by interfacial self-assembly. Journal of Colloid and Interface Science, 2010, 350, 58-62.	9.4	23
301	Effects of heavy phosphorus-doping on mechanical properties of Czochralski silicon. Journal of Applied Physics, 2010, 107, 123503.	2.5	23
302	Modulation of atomic-layer-deposited Al2O3 film passivation of silicon surface by rapid thermal processing. Applied Physics Letters, 2011, 99, .	3.3	23
303	One-dimensional hybrid nanostructures: synthesis via layer-by-layer assembly and applications. Nanoscale, 2012, 4, 5517.	5.6	23
304	Magnetic-fluorescent nanohybrids of carbon nanotubes coated with Eu, Gd Co-doped LaF3 as a multimodal imaging probe. Journal of Colloid and Interface Science, 2012, 367, 61-66.	9.4	23
305	Synthesis of NixSiy–SiGe core–shell nanowire arrays on Ni foam as a high-performance anode for Li-ion batteries. RSC Advances, 2013, 3, 7713.	3.6	23
306	Synthesis of SiGe-based three-dimensional nanoporous electrodes for high performance lithium-ion batteries. Journal of Power Sources, 2013, 229, 185-189.	7.8	23

#	Article	IF	CITATIONS
307	Highly Pure and Luminescent Graphene Quantum Dots on Silicon Directly Grown by Chemical Vapor Deposition. Particle and Particle Systems Characterization, 2016, 33, 8-14.	2.3	23
308	Density functional theory study on the B doping and B/P codoping of Si nanocrystals embedded in <mml:math xmlns:mml="http://www.w3.org/1998/Math/MathML"&gt; <mml:mrow> <mml:mi>Si</mml:mi> <mml:msub> <mml:mi mathvariant="normal"&gt;O <mml:mn>2</mml:mn> </mml:mi </mml:msub> </mml:mrow> .</mml:math 	3.2	23
309	Physical Review B, 2017, 95, . Promoting Effect of Si–OH on the Decomposition of Electrolytes in Lithium-Ion Batteries. Chemistry of Materials, 2020, 32, 6365-6373.	6.7	23
310	New Insight into the Metal-Catalyst-Free Direct Chemical Vapor Deposition Growth of Graphene on Silicon Substrates. Journal of Physical Chemistry C, 2021, 125, 1774-1783.	3.1	23
311	Oxygen-related centers in multicrystalline silicon. Solar Energy Materials and Solar Cells, 2000, 62, 37-42.	6.2	22
312	Defects in germanium-doped Czochralski silicon. Physica Status Solidi (A) Applications and Materials Science, 2005, 202, 931-938.	1.8	22
313	347nm ultraviolet electroluminescence from MgxZn1â^'xO-based light emitting devices. Applied Physics Letters, 2007, 90, 251115.	3.3	22
314	Reductive hydrothermal synthesis of La(OH)3:Tb3+ nanorods as a new green emitting phosphor. Journal of Nanoparticle Research, 2008, 10, 307-312.	1.9	22
315	Noninjection Synthesis of CdS and Alloyed CdSxSe1â^'x Nanocrystals Without Nucleation Initiators. Nanoscale Research Letters, 2010, 5, 966-971.	5.7	22
316	The effect of impurity-induced lattice strain and Fermi level position on low temperature oxygen diffusion in silicon. Journal of Applied Physics, 2011, 109, .	2.5	22
317	Efficiency improvement of silicon solar cells enabled by ZnO nanowhisker array coating. Nanoscale Research Letters, 2012, 7, 306.	5.7	22
318	Efficiency improvement of crystalline silicon solar cells with a back-surface field produced by boron and aluminum co-doping. Scripta Materialia, 2012, 66, 394-397.	5.2	22
319	Fabrication of TiO2 nanorod array/semiconductor nanocrystal hybrid structure for photovoltaic applications. Solar Energy, 2012, 86, 1359-1365.	6.1	22
320	Firmly bonded graphene–silicon nanocomposites as high-performance anode materials for lithium-ion batteries. RSC Advances, 2015, 5, 46173-46180.	3.6	22
321	Electroluminescence from metal-oxide-semiconductor devices with erbium-doped CeO2 films on silicon. Applied Physics Letters, 2015, 106, .	3.3	22
322	Surface plasmon enhanced luminescence from organic-inorganic hybrid perovskites. Applied Physics Letters, 2017, 110, 233113.	3.3	22
323	Progress of Graphene–Silicon Heterojunction Photovoltaic Devices. Advanced Materials Interfaces, 2018, 5, 1801520.	3.7	22
324	Towards green antisolvent for efficient CH3NH3PbBr3 perovskite light emitting diodes: A comparison of toluene, chlorobenzene, and ethyl acetate. Applied Physics Letters, 2019, 115, .	3.3	22

#	Article	IF	CITATIONS
325	A review on graphene-silicon Schottky junction interface. Journal of Alloys and Compounds, 2019, 806, 63-70.	5.5	22
326	Micro-defects in Ge doped Czochralski grown Si crystals. Journal of Crystal Growth, 2006, 292, 266-271.	1.5	21
327	Synthesis and characterization of single crystalline MnOOH and MnO2 nanorods by means of the hydrothermal process assisted with CTAB. Materials Letters, 2006, 60, 3895-3898.	2.6	21
328	Fabrication and characterization of CuInS2 films by chemical bath deposition in acid conditions. Journal of Materials Science: Materials in Electronics, 2009, 20, 609-613.	2.2	21
329	Microcrystalline silicon carbide thin films grown by HWCVD at different filament temperatures and their application in n-i-p microcrystalline silicon solar cells. Thin Solid Films, 2009, 517, 3513-3515.	1.8	21
330	Electrically pumped ultraviolet random lasing from ZnO-based metal-insulator-semiconductor devices: Dependence on carrier transport. Optics Express, 2009, 17, 4712.	3.4	21
331	Enhancement of electroluminescence from TiO2/p+-Si heterostructure-based devices through engineering of oxygen vacancies in TiO2. Applied Physics Letters, 2009, 95, .	3.3	21
332	Remarkable decrease in threshold for electrically pumped random ultraviolet lasing from ZnO film by incorporation of Zn_2TiO_4 nanoparticles. Optics Express, 2011, 19, 8662.	3.4	21
333	Density functional theory study on organically surface-modified silicene. RSC Advances, 2015, 5, 33831-33837.	3.6	21
334	Facile synthesis of Pd@Ru nanoplates with controlled thickness as efficient catalysts for hydrogen evolution reaction. CrystEngComm, 2018, 20, 4230-4236.	2.6	21
335	Wet-chemical synthesized MCMB@Si@C microspheres for high-performance lithium-ion battery anodes. Chemical Communications, 2018, 54, 9466-9469.	4.1	21
336	Building a Bridge from Papermaking to Solar Fuels. Angewandte Chemie - International Edition, 2019, 58, 14850-14854.	13.8	21
337	Intermetallic Pd <sub>3</sub> Pb square nanoplates as highly efficient electrocatalysts for oxygen reduction reaction. CrystEngComm, 2019, 21, 290-296.	2.6	21
338	Allâ€Earthâ€Abundant Photothermal Silicon Platform for CO <sub>2</sub> Catalysis with Nearly 100% Sunlight Harvesting Ability. Solar Rrl, 2021, 5, 2000387.	5.8	21
339	Low-temperature processed tantalum/niobium co-doped TiO <sub>2</sub> electron transport layer for high-performance planar perovskite solar cells. Nanotechnology, 2021, 32, 245201.	2.6	21
340	Stable and wide-wavelength tunable luminescence of CsPbX <sub>3</sub> nanocrystals encapsulated in metal–organic frameworks. Journal of Materials Chemistry C, 2022, 10, 5550-5558.	5.5	21
341	A simple and novel low-temperature hydrothermal synthesis of ZnO nanorods. Inorganic Materials, 2006, 42, 1210-1214.	0.8	20
342	Electron-beam-induced current study of grain boundaries in multicrystalline Si. Physica Status Solidi C: Current Topics in Solid State Physics, 2007, 4, 2908-2917.	0.8	20

#	Article	IF	CITATIONS
343	Improved fracture strength of multicrystalline silicon by germanium doping. Journal of Crystal Growth, 2011, 318, 230-233.	1.5	20
344	Improved cyclic stability of Mg2Si by direct carbon coating as anode materials for lithium-ion batteries. Journal of Alloys and Compounds, 2014, 587, 807-811.	5.5	20
345	Interface engineering and efficiency improvement of monolayer graphene–silicon solar cells by inserting an ultra-thin LiF interlayer. RSC Advances, 2015, 5, 46480-46484.	3.6	20
346	Illuminationâ€Induced Hole Doping for Performance Improvement of Graphene/nâ€Silicon Solar Cells with P3HT Interlayer. Advanced Electronic Materials, 2017, 3, 1600516.	5.1	20
347	Designing functional Σ13 grain boundaries at seed junctions for high-quality cast quasi-single crystalline silicon. Solar Energy Materials and Solar Cells, 2019, 200, 109985.	6.2	20
348	Effect of rapid thermal process on oxygen precipitation and denuded zone in nitrogen-doped silicon wafers. Microelectronic Engineering, 2003, 69, 97-104.	2.4	19
349	Aligned single crystal MgB2nanowires. Superconductor Science and Technology, 2004, 17, L31-L33.	3.5	19
350	Tiny SiO2 nano-wires synthesized on Si wafer. Physica E: Low-Dimensional Systems and Nanostructures, 2004, 23, 1-4.	2.7	19
351	Some critical factors in the synthesis of CdS nanorods by hydrothermal process. Materials Letters, 2005, 59, 3037-3041.	2.6	19
352	Copper precipitation in large-diameter Czochralski silicon. Journal of Applied Physics, 2005, 97, 094909.	2.5	19
353	Impurity engineering of Czochralski silicon used for ultra large-scaled-integrated circuits. Journal of Crystal Growth, 2009, 311, 837-841.	1.5	19
354	Enhanced electroluminescence of silicon-rich silicon nitride light-emitting devices by NH3 plasma and annealing treatment. Physica E: Low-Dimensional Systems and Nanostructures, 2009, 41, 920-922.	2.7	19
355	Electrochemical synthesis of SnCo alloy shells on orderly rod-shaped Cu current collectors as anode materials for lithium-ion batteries with enhanced performance. Journal of Alloys and Compounds, 2013, 570, 119-124.	5.5	19
356	Two-peak characteristic distribution of iron impurities at the bottom of cast quasi-single-crystalline silicon ingot. Scripta Materialia, 2013, 68, 655-657.	5.2	19
357	Experimental evidence of staggered oxygen dimers as a component of boron-oxygen complexes in silicon. Applied Physics Letters, 2013, 102, .	3.3	19
358	Structures, Oxidation, and Charge Transport of Phosphorusâ€Doped Germanium Nanocrystals. Particle and Particle Systems Characterization, 2016, 33, 271-278.	2.3	19
359	Electroluminescence from silicon-based light-emitting devices with erbium-doped TiO2 films annealed at different temperatures. Journal of Applied Physics, 2017, 122, .	2.5	19
360	Wetting Behavior of Metal-Catalyzed Chemical Vapor Deposition-Grown One-Dimensional Cubic-SiC Nanostructures. Langmuir, 2018, 34, 5214-5224.	3.5	19

#	Article	IF	CITATIONS
361	Silicon-based optoelectronic synaptic devices*. Chinese Physics B, 2020, 29, 070703.	1.4	19
362	Direct Growth of Graphene Nanowalls on Silicon Using Plasma-Enhanced Atomic Layer Deposition for High-Performance Si-Based Infrared Photodetectors. ACS Applied Electronic Materials, 2021, 3, 5048-5058.	4.3	19
363	CVD Graphene on Textured Silicon: An Emerging Technologically Versatile Heterostructure for Energy and Detection Applications. Advanced Materials Interfaces, 2022, 9, .	3.7	19
364	Intrinsic gettering Based on rapid thermal annealing in germanium-doped Czochralski silicon. Journal of Applied Physics, 2007, 101, 033526.	2.5	18
365	Bidirectional direct-current electroluminescence from i-MgxZn1â^'xO/n-ZnO/SiOx double-barrier heterostructures on Si. Applied Physics Letters, 2009, 94, .	3.3	18
366	Crystallization behaviors of TiO2 films derived from thermal oxidation of evaporated and sputtered titanium films. Journal of Alloys and Compounds, 2009, 480, 938-941.	5.5	18
367	Enhancement of room temperature dislocation-related photoluminescence of electron irradiated silicon. Journal of Applied Physics, 2013, 113, .	2.5	18
368	Formation of Various Pyramidal Structures on Monocrystalline Silicon Surface and Their Influence on the Solar Cells. Journal of Nanomaterials, 2013, 2013, 1-5.	2.7	18
369	Room temperature ferromagnetism of amorphous MgO films prepared by pulsed laser deposition. Applied Physics A: Materials Science and Processing, 2014, 115, 997-1001.	2.3	18
370	Self-generation of a quasi p–n junction for high efficiency chemical-doping-free graphene/silicon solar cells using a transition metal oxide interlayer. Journal of Materials Chemistry A, 2016, 4, 10558-10565.	10.3	18
371	Enhanced optoelectronic quality of perovskite films with excess CH <sub>3</sub> NH <sub>3</sub> I for high-efficiency solar cells in ambient air. Nanotechnology, 2017, 28, 205401.	2.6	18
372	Light-induced beneficial ion accumulation for high-performance quasi-2D perovskite solar cells. Energy and Environmental Science, 2022, 15, 2499-2507.	30.8	18
373	Effect of nitrogen on denuded zone in Czochralski silicon wafer. Semiconductor Science and Technology, 2004, 19, 548-551.	2.0	17
374	Sub-2 nm SnO2 nanocrystals: A reduction/oxidation chemical reaction synthesis and optical properties. Materials Research Bulletin, 2008, 43, 3164-3170.	5.2	17
375	Oxygen precipitation heterogeneously nucleating on silicon phosphide precipitates in heavily phosphorus-doped Czochralski silicon. Journal of Applied Physics, 2009, 105, 093503.	2.5	17
376	On the assumed impact of germanium doping on void formation in Czochralski-grown silicon. Journal of Applied Physics, 2010, 108, 123501.	2.5	17
377	Electrically pumped wavelength-tunable ultraviolet random lasing from Mg_xZn_1-xO films on Si. Optics Express, 2010, 18, 10668.	3.4	17
378	Growth and photoelectrochemical properties of ordered CuInS2 nanorod arrays. Chemical Communications, 2012, 48, 4746.	4.1	17

#	Article	IF	CITATIONS
379	Controlled synthesis of luminescent CuInS2 nanocrystals and their optical properties. Journal of Luminescence, 2012, 132, 313-317.	3.1	17
380	Simple synthesis of SiGe@C porous microparticles as high-rate anode materials for lithium-ion batteries. RSC Advances, 2017, 7, 33837-33842.	3.6	17
381	Light-emitting diodes based on colloidal silicon quantum dots. Journal of Semiconductors, 2018, 39, 061008.	3.7	17
382	Single Crystal Perovskite Microplate for Highâ€Order Multiphoton Excitation. Small Methods, 2019, 3, 1900396.	8.6	17
383	Controlling dislocation gliding and propagation in quasi-single crystalline silicon by using <110>-oriented seeds. Solar Energy Materials and Solar Cells, 2019, 193, 214-218.	6.2	17
384	Enhanced electrochemical properties of Cu3Si-embedded three-dimensional porous Si synthesized by one-pot synthesis. Journal of Alloys and Compounds, 2019, 792, 341-347.	5.5	17
385	Ion-templated fabrication of Pt-Cu alloy octahedra with controlled compositions for electrochemical detection of H2O2. Journal of Alloys and Compounds, 2019, 788, 1334-1340.	5.5	17
386	CsPbBr <sub>3</sub> quantum dots assisted crystallization of solution-processed perovskite films with preferential orientation for high performance perovskite solar cells. Nanotechnology, 2020, 31, 085401.	2.6	17
387	Unexpected Kirkendall effect in twinned icosahedral nanocrystals driven by strain gradient. Nano Research, 2020, 13, 2641-2649.	10.4	17
388	Silicon-based inorganic-organic hybrid optoelectronic synaptic devices simulating cross-modal learning. Science China Information Sciences, 2021, 64, 1.	4.3	17
389	A Review on Metastable Silicon Allotropes. Materials, 2021, 14, 3964.	2.9	17
390	The role of O2 in CdSeTe thin film deposition and CdSeTe/CdTe solar cell performance. Solar Energy Materials and Solar Cells, 2020, 214, 110595.	6.2	17
391	Control of the formation and luminescent properties of polymorphic erbium silicates on silicon. Optical Materials Express, 2019, 9, 1716.	3.0	17
392	Nitrogen-Oxygen Complexes in Silicon. Physica Status Solidi (B): Basic Research, 1998, 210, 295-299.	1.5	16
393	Crystallization and Raman Shift of Array-Orderly Silicon Nanowires after Annealing at High Temperature. Japanese Journal of Applied Physics, 2004, 43, 4460-4461.	1.5	16
394	Sulfide-assisted growth of silicon nano-wires by thermal evaporation of sulfur powders. Physica E: Low-Dimensional Systems and Nanostructures, 2004, 24, 278-281.	2.7	16
395	Hydrothermal synthesis and characterization of novel aloe-like SnS2 nanostructures. Journal of Materials Science, 2006, 41, 3489-3492.	3.7	16
396	Ge-vacancy pair in Ge-doped Czochralski silicon. Journal of Applied Physics, 2008, 103, .	2.5	16

#	Article	IF	CITATIONS
397	Phase-controlled synthesis of nickel silicide nanostructures. Materials Research Bulletin, 2012, 47, 3797-3803.	5.2	16
398	Electrically pumped random lasing from hydrothermal ZnO films of large grains. Applied Surface Science, 2015, 332, 620-624.	6.1	16
399	Silver–nickel oxide core–shell nanoflower arrays as high-performance anode for lithium-ion batteries. Journal of Power Sources, 2015, 285, 131-136.	7.8	16
400	Room-temperature processed, air-stable and highly efficient graphene/silicon solar cells with an organic interlayer. Journal of Materials Chemistry A, 2016, 4, 11284-11291.	10.3	16
401	Grain boundary engineering of high performance multicrystalline silicon: Control of iron contamination at the ingot edge. Solar Energy Materials and Solar Cells, 2017, 171, 131-135.	6.2	16
402	Intermetallic Pd <sub>3</sub> Pb ultrathin nanoplate-constructed flowers with low-coordinated edge sites boost oxygen reduction performance. Nanoscale, 2019, 11, 17301-17307.	5.6	16
403	Toward Waferâ€Scale Production of 2D Transition Metal Chalcogenides. Advanced Electronic Materials, 2021, 7, 2100278.	5.1	16
404	Electroluminescence from light-emitting devices based on erbium-doped ZnO/n-Si heterostructures: Enhancement effect of fluorine co-doping. Optics Express, 2019, 27, 30919.	3.4	16
405	Graphene/Si Heterostructure with an Organic Interfacial Layer for a Self-Powered Photodetector with a High ON/OFF Ratio. ACS Applied Electronic Materials, 2022, 4, 1715-1722.	4.3	16
406	Effect of heat treatment on carbon in multicrystalline silicon. Solar Energy Materials and Solar Cells, 2002, 72, 541-549.	6.2	15
407	Hydrogen annealing of grown-in voids in nitrogen-doped Czochralski grown silicon. Semiconductor Science and Technology, 2003, 18, 399-403.	2.0	15
408	Influence of copper precipitation on oxygen precipitation in Czochralski silicon. Semiconductor Science and Technology, 2004, 19, 299-305.	2.0	15
409	Annealing and amorphous silicon passivation of porous silicon with blue light emission. Applied Surface Science, 2005, 252, 1065-1069.	6.1	15
410	Effect of annealing on photoluminescence of passivated porous silicon. Solid-State Electronics, 2006, 50, 1529-1531.	1.4	15
411	Impurity engineering for germaniumâ€doped Czochralski silicon wafer used for ultra large scale integrated circuit. Physica Status Solidi C: Current Topics in Solid State Physics, 2009, 6, 625-632.	0.8	15
412	Chemical synthesis of Cu(In) metal inks to prepare CuInS2 thin films and solar cells. Journal of Alloys and Compounds, 2010, 507, 317-321.	5.5	15
413	Size controllable synthesis of ultrafine silver particles through a one-step reaction. Materials Letters, 2011, 65, 628-631.	2.6	15
414	Lightly boron and phosphorus co-doped silicon nanocrystals. Journal of Nanoparticle Research, 2012, 14, 1.	1.9	15

#	Article	IF	CITATIONS
415	Effect of dopant compensation on the performance of Czochralski silicon solar cells. Solar Energy Materials and Solar Cells, 2012, 101, 102-106.	6.2	15
416	Low-cost fabrication of Cu2ZnSnS4 thin films for solar cell absorber layers. Journal of Materials Science: Materials in Electronics, 2013, 24, 548-552.	2.2	15
417	Facile synthesis of high-quality Pt nanostructures with a controlled aspect ratio for methanol electro-oxidation. CrystEngComm, 2014, 16, 8340-8343.	2.6	15
418	Porous Si@C coaxial nanotubes: layer-by-layer assembly on ZnO nanorod templates and application to lithium-ion batteries. CrystEngComm, 2017, 19, 1220-1229.	2.6	15
419	Al2O3-Interlayer-Enhanced Performance of All-Inorganic Silicon-Quantum-Dot Near-Infrared Light-Emitting Diodes. IEEE Transactions on Electron Devices, 2018, 65, 577-583.	3.0	15
420	Precise Fabrication of Point Defects in Self-Assembled Three-Dimensional Macroporous Photonic Crystals. Journal of Physical Chemistry B, 2006, 110, 1107-1110.	2.6	14
421	Germanium effect on as-grown oxygen precipitation in Czochralski silicon. Journal of Crystal Growth, 2006, 291, 66-71.	1.5	14
422	Cathodoluminescence and its mapping of flower-like ZnO, ZnO/ZnS core–shell and tube-like ZnS nanostructures. Materials Research Bulletin, 2007, 42, 1286-1292.	5.2	14
423	Electroluminescence from TiO2/p+-Si heterostructure. Applied Physics Letters, 2009, 94, .	3.3	14
424	Effect of oxygen precipitates on dislocation motion in Czochralski silicon. Journal of Crystal Growth, 2010, 312, 169-173.	1.5	14
425	Electrically pumped ultraviolet random lasing from ZnO films: Compensation between optical gain and light scattering. Applied Physics Letters, 2010, 97, .	3.3	14
426	Electrically tunable electroluminescence from SiNx-based light-emitting devices. Optics Express, 2012, 20, 17359.	3.4	14
427	Light-induced degradation in n-type Czochralski silicon by boron-doping and thermal donor compensation. Journal of Applied Physics, 2012, 112, 084509.	2.5	14
428	Impact of rapid thermal processing on oxygen precipitation in heavily arsenic and antimony doped Czochralski silicon. Journal of Applied Physics, 2013, 113, 163510.	2.5	14
429	Fabrication and photovoltaic conversion enhancement of graphene/n-Si Schottky barrier solar cells by electrophoretic deposition. Electrochimica Acta, 2014, 130, 279-285.	5.2	14
430	Facile synthesis of PtCu <sub>3</sub> alloy hexapods and hollow nanoframes as highly active electrocatalysts for methanol oxidation. CrystEngComm, 2016, 18, 7823-7830.	2.6	14
431	All-vacuum deposited and thermally stable perovskite solar cells with F4-TCNQ/CuPc hole transport layer. Nanotechnology, 2020, 31, 065401.	2.6	14
432	Investigation on the light and elevated temperature induced degradation of gallium-doped Cz-Si. Solar Energy, 2021, 225, 407-411.	6.1	14

#	Article	IF	CITATIONS
433	Cesium-lead-bromide perovskites with balanced stoichiometry enabled by sodium-bromide doping for all-vacuum deposited silicon-based light-emitting diodes. Journal of Materials Chemistry C, 2021, 9, 2016-2023.	5.5	14
434	Perovskite-Enhanced Silicon-Nanocrystal Optoelectronic Synaptic Devices for the Simulation of Biased and Correlated Random-Walk Learning. Research, 2020, 2020, 7538450.	5.7	14
435	Synergistic effects of bithiophene ammonium salt for high-performance perovskite solar cells. Journal of Materials Chemistry A, 2022, 10, 9971-9980.	10.3	14
436	Crystallization of amorphous silicon thin films: The effect of rapid thermal processing pretreatment. Vacuum, 2006, 80, 415-420.	3.5	13
437	Investigation of intrinsic gettering for germanium doped Czochralski silicon wafer. Journal of Applied Physics, 2007, 101, 113512.	2.5	13
438	Optical properties of single-phase β-FeSi2 films fabricated by electron beam evaporation. Applied Surface Science, 2008, 254, 4875-4878.	6.1	13
439	Microcrystalline siliconâ€carbon alloys as antiâ€reflection window layers in high efficiency thin film silicon solar cells. Physica Status Solidi - Rapid Research Letters, 2008, 2, 160-162.	2.4	13
440	Magnesium catalyzed growth of SiO2hierarchical nanostructures by a thermal evaporation process. Nanotechnology, 2008, 19, 165601.	2.6	13
441	Highly Conductive p-Type Silicon Carbon Alloys Deposited by Hot-Wire Chemical Vapor Deposition. Japanese Journal of Applied Physics, 2010, 49, 041303.	1.5	13
442	Immobilization of dislocations by oxygen precipitates in Czochralski silicon: Feasibility of precipitation strengthening mechanism. Journal of Crystal Growth, 2011, 324, 93-97.	1.5	13
443	Development of microcrystalline silicon carbide window layers by hot-wire CVD and their applications in microcrystalline silicon thin film solar cells. Thin Solid Films, 2011, 519, 4523-4526.	1.8	13
444	Effects of excess silicon on the 1540 nm Er3+ luminescence in silicon rich oxynitride films. Applied Physics Letters, 2013, 103, .	3.3	13
445	Electroluminescence from light-emitting devices with erbium-doped TiO <sub>2</sub> films: Enhancement effect of yttrium codoping. Journal of Applied Physics, 2016, 120, 163104.	2.5	13
446	An industrial solution to light-induced degradation of crystalline silicon solar cells. Frontiers in Energy, 2017, 11, 67-71.	2.3	13
447	Effects of oxygen related thermal donors on the performance of silicon heterojunction solar cells. Solar Energy Materials and Solar Cells, 2018, 179, 17-21.	6.2	13
448	Multicrystalline silicon assisted by polycrystalline silicon slabs as seeds. Solar Energy Materials and Solar Cells, 2018, 179, 312-318.	6.2	13
449	Interface engineering of C60/ fluorine doped tin oxide on the photovoltaic performance of perovskite solar cells using the physical vapor deposition technique. Journal Physics D: Applied Physics, 2019, 52, 225104.	2.8	13
450	Origin of Plasticity in Nanostructured Silicon. Physical Review Letters, 2020, 124, 185701.	7.8	13

#	Article	IF	CITATIONS
451	Facile synthesis of ternary PtPdCu alloy hexapods as highly efficient electrocatalysts for methanol oxidation. RSC Advances, 2020, 10, 12689-12694.	3.6	13
452	A unique ligand effect in Pt-based core–shell nanocubes to boost oxygen reduction electrocatalysis. Journal of Materials Chemistry A, 2021, 9, 22653-22659.	10.3	13
453	Electronic and Optical Properties of Threading Dislocations in <i>n</i> -Type 4H-SiC. ACS Applied Electronic Materials, 2022, 4, 1678-1683.	4.3	13
454	Thermal acceptor formation in nitrogenâ€doped silicon. Applied Physics Letters, 1991, 59, 1227-1229.	3.3	12
455	Infrared absorption of nitrogen–oxygen complex in silicon. Materials Science and Engineering B: Solid-State Materials for Advanced Technology, 2000, 72, 121-123.	3.5	12
456	Influence of oxygen precipitates on the warpage of annealed silicon wafers. Microelectronic Engineering, 2003, 66, 345-351.	2.4	12
457	Effect of post-treatment processes on the photoluminescence of porous silicon. Physica B: Condensed Matter, 2005, 364, 180-185.	2.7	12
458	Effect of light germanium doping on thermal donors in Czochralski silicon wafers. Materials Science in Semiconductor Processing, 2006, 9, 110-113.	4.0	12
459	Surface synthesis of PbS nanoparticles on silica spheres by a sonochemical approach. Journal of Materials Science, 2007, 42, 1376-1380.	3.7	12
460	Effect of germanium on the kinetics of boron-oxygen defect generation and dissociation in Czochralski silicon. Applied Physics Letters, 2010, 97, 162107.	3.3	12
461	Density functional theory study on a 1.4 nm silicon nanocrystal coated with carbon. RSC Advances, 2012, 2, 11227.	3.6	12
462	A chemical strategy to reinforce electrically pumped ultraviolet random lasing from ZnO films. Journal of Materials Chemistry, 2012, 22, 16738.	6.7	12
463	Towards thinner and low bowing silicon solar cells: form the boron and aluminum coâ€doped back surface field with thinner metallization film. Progress in Photovoltaics: Research and Applications, 2013, 21, 456-461.	8.1	12
464	Energy transfer from luminescent centers to Er3+ in erbium-doped silicon-rich oxide films. Nanoscale Research Letters, 2013, 8, 366.	5.7	12
465	Light-emitting devices based on erbium-doped TiO2/ <i>p</i> +-Si heterostructures: Engineering of electroluminescence via aluminum co-doping. Applied Physics Letters, 2013, 102, .	3.3	12
466	Doping Silicon Wafers with Boron by Use of Silicon Paste. Journal of Materials Science and Technology, 2013, 29, 652-654.	10.7	12
467	Evolution of electroluminescence from silicon nitride light-emitting devices via nanostructural silver. Nanoscale, 2013, 5, 3435.	5.6	12
468	Constructing Ag nanoparticles–single wall carbon hybrid nanostructure to improve field emission properties. Applied Surface Science, 2013, 265, 187-191.	6.1	12

#	Article	IF	CITATIONS
469	Germanium-doped crystalline silicon: Effects of germanium doping on boron-related defects. Journal of Crystal Growth, 2014, 401, 141-145.	1.5	12
470	Color-tunable electroluminescence from Eu-doped TiO_2/p^+-Si heterostructured devices: engineering of energy transfer. Optics Express, 2015, 23, 2819.	3.4	12
471	Formation, Structures and Electronic Properties of Silicene Oxides on Ag(111). Journal of Materials Science and Technology, 2017, 33, 751-757.	10.7	12
472	Interface engineering of Graphene-Silicon heterojunction solar cells. Superlattices and Microstructures, 2016, 99, 3-12.	3.1	12
473	Formation, Stability, Geometry and Band Structure of Organically Surface-Modified Germanane. Journal of Materials Science and Technology, 2017, 33, 59-64.	10.7	12
474	Negatively charged silicon nitride films for improved p-type silicon surface passivation by low-temperature rapid thermal annealing. Journal Physics D: Applied Physics, 2019, 52, 345102.	2.8	12
475	A novel three-dimensional architecture of Co–Ge nanowires towards high-rate lithium and sodium storage. Journal of Alloys and Compounds, 2020, 815, 152281.	5.5	12
476	Polarized Laser Switching with Giant Contrast in MOFâ€Based Mixedâ€Matrix Membrane. Advanced Science, 2022, 9, e2200953.	11.2	12
477	Effect of nitrogen doping on the minority carrier lifetime in Czochralski silicon. Microelectronic Engineering, 2003, 66, 373-378.	2.4	11
478	Silicon nano-wires fabricated by thermal evaporation of silicon wafer. Physica E: Low-Dimensional Systems and Nanostructures, 2004, 24, 268-271.	2.7	11
479	Transformation mechanism of Te particles into Te nanotubes and nanowires during solvothermal process. Journal of Crystal Growth, 2006, 289, 568-573.	1.5	11
480	Infrared spectra of silicon nanowires. Materials Letters, 2007, 61, 894-896.	2.6	11
481	The optical properties of porous silicon produced by metal-assisted anodic etching. Journal of Materials Science, 2007, 42, 8496-8500.	3.7	11
482	Enhanced photoluminescence of Tb3+ in SnO2 film by phosphorus diffusion process. Journal of Alloys and Compounds, 2009, 474, 246-249.	5.5	11
483	Effect of rapid thermal annealing on photoluminescence and crystal structures of CdZnO films. Journal of Crystal Growth, 2010, 312, 1908-1911.	1.5	11
484	Optical absorption and emission of nitrogen-doped silicon nanocrystals. Nanoscale, 2011, 3, 4584.	5.6	11
485	Cobalt–iron cyanide hollow cubes: Three-dimensional self-assembly and magnetic properties. Journal of Alloys and Compounds, 2011, 509, 8382-8386.	5.5	11
486	Improvement in the mechanical performance of Czochralski silicon under indentation by germanium doping. Scripta Materialia, 2011, 64, 832-835.	5.2	11

DEREN YANG

#	Article	IF	CITATIONS
487	Solvothermal synthesis of carbon-coated tin nanorods for superior reversible lithium ion storage. Materials Research Bulletin, 2011, 46, 2278-2282.	5.2	11
488	Light absorption enhancement of amorphous silicon film coupled with metal nanoshells. Journal of the Optical Society of America B: Optical Physics, 2013, 30, 405.	2.1	11
489	Near-infrared electroluminescence from light-emitting devices based on Nd-doped TiO2/ <i>p</i> +-Si heterostructures. Applied Physics Letters, 2014, 104, .	3.3	11
490	Green electroluminescence from Tb4O7 films on silicon: Impact excitation of Tb3+ ions by hot carriers. Applied Physics Letters, 2016, 108, .	3.3	11
491	One-Pot Fast Synthesis of Leaf-Like CuO Nanostructures and CuO/Ag Microspheres with Photocatalytic Application. Nano, 2017, 12, 1750035.	1.0	11
492	Plasmon-Coupled Förster Resonance Energy Transfer between Silicon Quantum Dots. Journal of Physical Chemistry C, 2019, 123, 23604-23609.	3.1	11
493	Twoâ€Dimensional Silicon for (Photo)Catalysis. Solar Rrl, 2021, 5, 2000392.	5.8	11
494	Kinetics Study on Carrier Injectionâ€Induced Degradation and Regeneration at Elevated Temperature in pâ€Type Castâ€Monosilicon Passivated Emitter Rear Contact Solar Cells. Solar Rrl, 2021, 5, 2100035.	5.8	11
495	Thermal Warpage of Czochralski Silicon Wafers Grown under a Nitrogen Ambience. Physica Status Solidi A, 1998, 169, 193-198.	1.7	10
496	Nitrogen effect on self-interstitial generation in Czochralski silicon revealed by gold diffusion experiments. Journal of Applied Physics, 2001, 90, 3642-3644.	2.5	10
497	Oxygen in Czochralski silicon used for solar cells. Solar Energy Materials and Solar Cells, 2002, 72, 133-138.	6.2	10
498	Photoluminescence properties of the composite of porous alumina and poly (2,5-dibutoxy-1,4) Tj ETQq0 0 0 rgB	T /gverlocl	₹ 10 Tf 50 30
499	Effects of nitrogen doping on the dissolution of oxygen precipitates in Czochralski silicon during rapid thermal annealing. Semiconductor Science and Technology, 2004, 19, 715-719.	2.0	10
500	Effects of rapid thermal processing on oxygen precipitation in Czochralski silicon wafer. Semiconductor Science and Technology, 2004, 19, 630-633.	2.0	10
501	The effect of the ramping rate on oxygen precipitation and the denuded zone in heavily doped Czochralski silicon. Journal of Physics Condensed Matter, 2004, 16, 1539-1545.	1.8	10
502	Excitation transfer from porous silicon to polymer. Materials Science and Engineering B: Solid-State Materials for Advanced Technology, 2005, 121, 229-231.	3.5	10
503	Comment on "Electronic Transport, Structure, and Energetics of Endohedral Gd@C82 Metallofullerenes― Nano Letters, 2005, 5, 2340-2340.	9.1	10
504	Rapid-thermal-processing-based intrinsic gettering for nitrogen-doped Czochralski silicon. Journal of Applied Physics, 2005, 98, 084502.	2.5	10

#	Article	IF	CITATIONS
505	A novel low-temperature chemical solution route for straight and dendrite-like ZnO nanostructures. Materials Science and Engineering B: Solid-State Materials for Advanced Technology, 2007, 141, 76-81.	3.5	10
506	Aligned single crystal Al-catalyzed boron nanorods on Si substrates. European Physical Journal B, 2007, 56, 35-39.	1.5	10
507	Effect of silicon interstitials on Cu precipitation in n-type Czochralski silicon. Journal of Applied Physics, 2008, 103, .	2.5	10
508	Enhanced oxygen precipitation in neutron-irradiated nitrogen-doped Czochralski silicon crystal. Journal of Applied Physics, 2008, 104, .	2.5	10
509	Structure of Ge–O complexes in Czochralski silicon. Physica B: Condensed Matter, 2009, 404, 58-60.	2.7	10
510	The modulation of surface texture for single-crystalline Si solar cells using calibrated silver nanoparticles as a catalyst. Nanotechnology, 2011, 22, 025703.	2.6	10
511	Improved electroluminescence from silicon nitride light emitting devices by localized surface plasmons. Optical Materials Express, 2012, 2, 872.	3.0	10
512	Influence of the compensation level on the performance of p-type crystalline silicon solar cells: Theoretical calculations and experimental study. Solar Energy Materials and Solar Cells, 2012, 107, 263-271.	6.2	10
513	First-Principles Study of Interstitial Boron and Oxygen Dimer Complex in Silicon. Applied Physics Express, 2013, 6, 041301.	2.4	10
514	Synthesis of nanoporous three-dimensional current collector for high-performance lithium-ion batteries. RSC Advances, 2013, 3, 7543.	3.6	10
515	Ge@C three-dimensional porous particles as high-performance anode materials of lithium-ion batteries. RSC Advances, 2015, 5, 63056-63062.	3.6	10
516	Effects of n-butyl amine incorporation on the performance of perovskite light emitting diodes. Nanotechnology, 2019, 30, 105703.	2.6	10
517	Strain effect in Pd@PdAg twinned nanocrystals towards ethanol oxidation electrocatalysis. Nanoscale Advances, 2021, 4, 111-116.	4.6	10
518	Deformation of 4H-SiC: The role of dopants. Applied Physics Letters, 2022, 120, 052105.	3.3	10
519	Intrinsic gettering of Czochralski silicon annealed in argon and nitrogen atmosphere. Physica B: Condensed Matter, 2001, 307, 40-44.	2.7	9
520	Silicon nano-wires fabricated by a novel thermal evaporation of zinc sulfide. Physica E: Low-Dimensional Systems and Nanostructures, 2004, 24, 178-182.	2.7	9
521	Effect of carbon doping on oxygen precipitation behavior in internal gettering processing for Czochralski silicon. Journal of Crystal Growth, 2006, 290, 61-66.	1.5	9
522	Enhanced red electroluminescence from a polycrystalline diamond film/Si heterojunction structure. Applied Physics Letters, 2007, 90, 161123.	3.3	9

#	Article	IF	CITATIONS
523	Crystal-originated particles in germanium-doped Czochralski silicon crystal. Journal of Crystal Growth, 2007, 306, 262-268.	1.5	9
524	Hydrothermal Synthesis and Photoluminescence of Eu <sub>2â^'<i>x</i></sub> Sm <sub><i>x</i></sub> Sn <sub>2</sub> O <sub>7</sub> ( <i>x</i> = 0–2.0) Nanophosphors. Journal of Nanoscience and Nanotechnology, 2008, 8, 1427-1431.	0.9	9
525	Growth of In2O3 Nanowires Catalyzed by Cu via a Solid–Liquid–Solid Mechanism. Nanoscale Research Letters, 2010, 5, 898-903.	5.7	9
526	Electrically pumped ultraviolet random lasing from heterostructures formed by bilayered MgZnO films on silicon. Applied Physics Letters, 2010, 97, 061111.	3.3	9
527	Large-scale synthesis of water-soluble nanowires as versatile templates for nanotubes. Chemical Communications, 2011, 47, 1006-1008.	4.1	9
528	Cu–In intermetallic compound inks for CuInS2 solar cells. Journal of Materials Science: Materials in Electronics, 2011, 22, 1124-1129.	2.2	9
529	Sensitization of Er^3+ ions in silicon rich oxynitride films: effect of thermal treatments. Optics Express, 2014, 22, 13022.	3.4	9
530	Zn <sub>2</sub> GeO <sub>4</sub> @C Core–Shell Nanorods as Highly Reversible Anode Materials for Lithiumâ€lon Batteries. Energy Technology, 2017, 5, 1656-1662.	3.8	9
531	Influence of vertical temperature gradients on wafer quality and cell efficiency of Seed-assisted high-performance multi-crystalline silicon. Journal of Crystal Growth, 2017, 467, 65-70.	1.5	9
532	Suppress of dislocations induced by feedstocks weight in cast-mono crystalline silicon. Solar Energy, 2021, 223, 125-131.	6.1	9
533	NIR Light Driven Terahertz Wave Modulator with a Large Modulation Depth Based on a Siliconâ€PEDOT:PSSâ€Perovskite Hybrid System. Advanced Materials Technologies, 2020, 5, 1901090.	5.8	9
534	Anti-reflection effect of large-area ZnO nano-needle array on multi-crystalline silicon solar cells. Materials Science in Semiconductor Processing, 2022, 138, 106299.	4.0	9
535	Tuning the Photon Sensitization Mechanism in Metalâ€Halideâ€Perovskiteâ€Based Nanocomposite Films Toward Highly Efficient and Stable Xâ€Ray Detection. Advanced Optical Materials, 2022, 10, .	7.3	9
536	Revealing the Correlation of Light Soaking Effect with Ion Migration in Perovskite Solar Cells. Solar Rrl, 2022, 6, .	5.8	9
537	Numerical Simulation of a Novel Method for PVT Growth of SiC by Adding a Graphite Block. Crystals, 2021, 11, 1581.	2.2	9
538	Interlayer-Assisted Growth of Si-Based All-Inorganic Perovskite Films via Chemical Vapor Deposition for Sensitive and Stable X-ray Detection. Journal of Physical Chemistry Letters, 2022, 13, 5441-5450.	4.6	9
539	Shallow thermal donors in silicon doped with isotopic oxygen. Physica B: Condensed Matter, 2001, 302-303, 193-196.	2.7	8
540	Nickel precipitation in large-diameter Czochralski silicon. Physica B: Condensed Matter, 2004, 344, 407-412.	2.7	8

#	Article	IF	CITATIONS
541	Copper sulfide micro-tubes fabricated by thermal evaporation of zinc sulfide. Materials Letters, 2005, 59, 2094-2096.	2.6	8
542	Oxygen precipitation in neutron-irradiated Czochralski silicon annealed at elevated temperature. Physica Status Solidi A, 2005, 202, 2442-2447.	1.7	8
543	Germanium effect on oxygen-related defects in Czochralski silicon. Physica Status Solidi (A) Applications and Materials Science, 2006, 203, 685-695.	1.8	8
544	Defects in Ge-doped Cz-Si annealed under high stress. Materials Science in Semiconductor Processing, 2006, 9, 82-87.	4.0	8
545	Enhanced oxygen out-diffusion in silicon crystal doped with germanium. Journal of Applied Physics, 2007, 102, 066102.	2.5	8
546	The influence of microstructure on optical properties of porous silicon. Solid-State Electronics, 2007, 51, 678-682.	1.4	8
547	Controllable chemical reaction synthesis of Tb(OH)3 nanorods and their photoluminescence property. Materials Letters, 2009, 63, 1180-1182.	2.6	8
548	Effects of high temperature rapid thermal processing on oxygen precipitation in heavily arsenic-doped Czochralski silicon. Journal of Crystal Growth, 2011, 318, 183-186.	1.5	8
549	Silicon nanocrystals doped with substitutional or interstitial manganese. Applied Physics Letters, 2011, 99, 193108.	3.3	8
550	Simple Synthesis of Flower-Like <mml:math xmlns:mml="http://www.w3.org/1998/Math/MathML"&gt;<mml:mrow><mml:msub><mml:mrow><mml:mtext>ln<!--<br-->mathvariant="bold"&gt;2</mml:mtext></mml:mrow></mml:msub><mml:msub><mml:mrow><mml:mtext>Smathvariant="bold"&gt;3</mml:mtext></mml:mrow></mml:msub></mml:mrow><td></td><td></td></mml:math 		
551	Localized surface plasmon resonance enhanced photoluminescence from SiNx with different N/Si ratios. Optical Materials Express, 2012, 2, 1437.	3.0	8
552	The coupling between localized surface plasmons and excitons via Purcell effect. Nanoscale Research Letters, 2012, 7, 669.	5.7	8
553	Dislocation-related electroluminescence of silicon after electron irradiation. Solid State Communications, 2012, 152, 1956-1959.	1.9	8
554	Colloidal synthesis of monodisperse quaternary CuInSSe nanocrystals. Materials Chemistry and Physics, 2012, 132, 865-869.	4.0	8
555	Germanium-doped crystalline silicon: A new substrate for photovoltaic application. Journal of Crystal Growth, 2013, 362, 140-144.	1.5	8
556	<i>Ab initio</i> study on the effect of structural relaxation on the electronic and optical properties of P-doped Si nanocrystals. Journal of Applied Physics, 2014, 116, .	2.5	8
557	Ultraviolet-visible electroluminescence from metal-oxide-semiconductor devices with CeO2 films on silicon. AIP Advances, 2015, 5, 037107.	1.3	8
558	Sensitizing properties of luminescence centers on the emission of Er3+ in Si-rich SiO2 film. Journal of Applied Physics, 2016, 119, 203106.	2.5	8

#	Article	IF	CITATIONS
559	Core–shell and alloy integrating PdAu bimetallic nanoplates on reduced graphene oxide for efficient and stable hydrogen evolution catalysts. RSC Advances, 2017, 7, 43373-43379.	3.6	8
560	Determination of the Boron and Phosphorus Ionization Energies in Compensated Silicon by Temperature-Dependent Luminescence. Silicon, 2017, 9, 147-151.	3.3	8
561	Design and Photovoltaic Properties of Graphene/Silicon Solar Cell. Journal of Electronic Materials, 2018, 47, 5025-5032.	2.2	8
562	Hierarchical Carbon Shell Compositing Microscale Silicon Skeleton as High-Performance Anodes for Lithium-Ion Batteries. ACS Applied Energy Materials, 2021, 4, 4976-4985.	5.1	8
563	Understanding the Influence of Cation and Anion Migration on Mixedâ€Composition Perovskite Solar Cells via Transient Ion Drift. Physica Status Solidi - Rapid Research Letters, 2021, 15, 2100225.	2.4	8
564	Theoretical study on the improvement of the doping efficiency of Al in 4H-SiC by co-doping group-IVB elements. Chinese Physics B, 2022, 31, 046104.	1.4	8
565	Recent Progress on the Scanning Tunneling Microscopy and Spectroscopy Study of Semiconductor Heterojunctions. Small, 2021, , 2100655.	10.0	8
566	PdPtRu nanocages with tunable compositions for boosting the methanol oxidation reaction. Nanoscale Advances, 2022, 4, 1158-1163.	4.6	8
567	Compensation of <i>p</i> -type doping in Al-doped 4H-SiC. Journal of Applied Physics, 2022, 131, .	2.5	8
568	High-responsivity graphene/hyperdoped-silicon heterostructure infrared photodetectors. Optics and Laser Technology, 2022, 153, 108291.	4.6	8
569	Effect of annealing atmosphere on oxygen precipitation and formation of denuded zone in Czochralski silicon wafer. Physica Status Solidi (A) Applications and Materials Science, 2006, 203, 2370-2375.	1.8	7
570	Recombination behavior of nickel in cast multicrystalline silicon. Materials Science in Semiconductor Processing, 2006, 9, 304-307.	4.0	7
571	Growth of misfit dislocation-free p/p+ thick epitaxial silicon wafers on Ge–B-codoped substrates. Physica B: Condensed Matter, 2006, 376-377, 841-844.	2.7	7
572	The structural evolution of nanocrystalline diamond films synthesized by r.f. PECVD. Materials Letters, 2006, 60, 730-733.	2.6	7
573	Room temperature electroluminescence from a nanocrystalline diamond/Si heterojunction. Diamond and Related Materials, 2007, 16, 306-310.	3.9	7
574	Flower-like silicon nanostructures. Physica E: Low-Dimensional Systems and Nanostructures, 2007, 38, 27-30.	2.7	7
575	Controllable synthesis of uncapped metal nanoparticle assembly at the air–water interface. Materials Chemistry and Physics, 2008, 111, 271-274.	4.0	7
576	Oxygen precipitation in Czochralski silicon: Effect of ramped anneal from 300to750°C. Journal of Applied Physics, 2008, 103, 064911.	2.5	7

#	Article	IF	CITATIONS
577	Controllable growth of Se nanotubes and nanowires from different solvent during the sonochemical process. Materials Letters, 2009, 63, 1-4.	2.6	7
578	Rapid-thermal-anneal-based internal gettering forÂgermanium-doped Czochralski silicon. Applied Physics A: Materials Science and Processing, 2009, 94, 905-910.	2.3	7
579	Transmission electron microscopy investigation of the micro-defects in Czochralski silicon. Journal of Alloys and Compounds, 2009, 478, 758-762.	5.5	7
580	Electrophotoluminescence of sol-gel derived ZnO film: Effect of electric field on near-band-edge photoluminescence. Optics Express, 2009, 17, 11434.	3.4	7
581	Effect of vacancies on oxygen precipitation in germanium-doped Czochralski silicon. Journal of Applied Physics, 2010, 107, .	2.5	7
582	Single step synthesis of CdSeS nanorods with chemical composition gradients. Journal of Crystal Growth, 2010, 312, 3406-3409.	1.5	7
583	Quantification of characteristic parameters for the dissociation kinetics of iron–boron pairs in Czochralski silicon. Scripta Materialia, 2011, 64, 217-220.	5.2	7
584	Electron irradiation induced defects in germaniumâ€doped Czochralski silicon substrates and diodes. Physica Status Solidi C: Current Topics in Solid State Physics, 2011, 8, 674-677.	0.8	7
585	On the low carrier lifetime edge zone in multicrystalline silicon ingots. Journal of Applied Physics, 2014, 115, .	2.5	7
586	Oxygen precipitation in 1020 cmâ^'3 germanium-doped Czochralski silicon. Journal of Applied Physics, 2015, 117, 025705.	2.5	7
587	Silver-nickel oxide core-shell nanoparticle array electrode with enhanced lithium-storage performance. Electrochimica Acta, 2015, 174, 893-899.	5.2	7
588	Suppression of boron-oxygen defects in Czochralski silicon by carbon co-doping. Applied Physics Letters, 2015, 106, 102105.	3.3	7
589	A novel Co–Li <sub>2</sub> O@Si core–shell nanowire array composite as a high-performance lithium-ion battery anode material. Nanoscale, 2016, 8, 4511-4519.	5.6	7
590	Sample thickness effect of thermal vibration correction within X-ray dynamical theory for germanium-doped silicon. Journal of Applied Physics, 2017, 121, 125704.	2.5	7
591	Sensitized photoluminescence of erbium silicate synthesized on porous silicon framework. Journal of Applied Physics, 2017, 122, .	2.5	7
592	Growth and ripening of oxygen precipitation in neutron-irradiated Czochralski silicon. Materials Science in Semiconductor Processing, 2018, 74, 369-374.	4.0	7
593	Comparison on mechanical properties of heavily phosphorus- and arsenic-doped Czochralski silicon wafers. AIP Advances, 2018, 8, .	1.3	7
594	Structure and conductivity enhanced treble-shelled porous silicon as an anode for high-performance lithium-ion batteries. RSC Advances, 2019, 9, 35392-35400.	3.6	7

#	Article	IF	CITATIONS
595	Electroluminescence from metal–oxide–semiconductor devices based on erbium silicate nanocrystals and silicon nanocrystals co-embedded in silicon oxide thin films. Journal of Materials Science: Materials in Electronics, 2021, 32, 20659-20667.	2.2	7
596	Wet etching in β-Ga <sub>2</sub> O <sub>3</sub> bulk single crystals. CrystEngComm, 2022, 24, 1127-1144.	2.6	7
597	Enhanced electrocatalytic reduction of CO <sub>2</sub> to formate <i>via</i> doping Ce in Bi <sub>2</sub> O <sub>3</sub> nanosheets. Nanoscale Advances, 2022, 4, 2288-2293.	4.6	7
598	Transmission electron microscopic observation of oxygen precipitates in nitrogen-doped silicon. Microelectronic Engineering, 2001, 56, 205-208.	2.4	6
599	Transmission electron microscopy investigation of oxygen precipitation in Czochralski silicon annealed under high pressure. Materials Science and Engineering B: Solid-State Materials for Advanced Technology, 2003, 102, 84-87.	3.5	6
600	Oxidation-induced stacking faults and related grown-in oxygen precipitates in nitrogen-doped Czochralski silicon. Semiconductor Science and Technology, 2003, 18, 393-397.	2.0	6
601	Effect of high temperature–pressure on nitrogen-doped Czochralski silicon. Journal of Physics Condensed Matter, 2004, 16, 473-481.	1.8	6
602	Tiny silicon nano-wires synthesis on silicon wafers. Physica E: Low-Dimensional Systems and Nanostructures, 2004, 24, 328-332.	2.7	6
603	Defects in nitrogen-doped multicrystalline silicon. Physica B: Condensed Matter, 2004, 344, 1-4.	2.7	6
604	Thermal nitridation kinetics of silicon wafers in nitrogen atmosphere during annealing. Thin Solid Films, 2005, 474, 326-329.	1.8	6
605	Al-assisted Anodic Etched Porous Silicon. Journal of Materials Science, 2006, 41, 5283-5286.	3.7	6
606	Micro-characterisation of Si wafers by high-pressure thermopower technique. Physica B: Condensed Matter, 2006, 376-377, 177-180.	2.7	6
607	Influence of copper precipitation on the formation of denuded zone in Czochralski silicon. Journal of Applied Physics, 2007, 102, 114506.	2.5	6
608	A chromium-free etchant for delineation of defects in heavily doped n-type silicon wafers. Materials Science in Semiconductor Processing, 2008, 11, 131-136.	4.0	6
609	Photoluminescence of Tb3+-doped SiNx films with different Si concentrations. Materials Science and Engineering B: Solid-State Materials for Advanced Technology, 2008, 146, 126-130.	3.5	6
610	Microcrystalline silicon thin film solar cells with microcrystalline silicon carbide window layers and silicon absorber layers both prepared by Hotâ€Wire CVD. Physica Status Solidi - Rapid Research Letters, 2010, 4, 61-63.	2.4	6
611	Structural characterization of CuInS <sub>2</sub> thin films from Cu–In metal inks. Physica Status Solidi (A) Applications and Materials Science, 2011, 208, 2399-2405.	1.8	6
612	CdSe Quantum Dots Sensitized Mesoporous TiO <sub>2</sub> Solar Cells with CuSCN as Solid-State Electrolyte. Journal of Nanomaterials, 2011, 2011, 1-5.	2.7	6

#	Article	IF	CITATIONS
613	Grown-in precipitates in heavily phosphorus-doped Czochralski silicon. Journal of Applied Physics, 2012, 111, 033520.	2.5	6
614	Structure and magnetic properties of γ′-Fe4N films grown on MgO-buffered Si (001). Physica B: Condensed Matter, 2012, 407, 4783-4786.	2.7	6
615	Quantitative Study of the Evolution of Oxygen and Vacancy Complexes in Czochralski Silicon. Applied Physics Express, 2012, 5, 021302.	2.4	6
616	Influence of defects and impurities on the deteriorated border region in multicrystalline silicon ingots. Crystal Research and Technology, 2012, 47, 7-12.	1.3	6
617	Modulation effect of microstructures in silicon-rich oxide matrix on photoluminescence from silicon nanoclusters prepared by different fabrication techniques. Applied Physics A: Materials Science and Processing, 2013, 113, 121-126.	2.3	6
618	Tailoring Effect of Enhanced Local Electric Field From Metal Nanoparticles on Electroluminescence of Silicon-Rich Silicon Nitride. IEEE Journal of Selected Topics in Quantum Electronics, 2013, 19, 4602504-4602504.	2.9	6
619	Study on permanent deactivation of the light-induced degradation in p-type compensated crystalline silicon solar cells. Solar Energy Materials and Solar Cells, 2013, 117, 29-33.	6.2	6
620	Comparison on electrically pumped random laser actions of hydrothermal and sputtered ZnO films. Journal of Applied Physics, 2013, 114, .	2.5	6
621	Improving the Solar Cell Module Performance by a Uniform Porous Antireflection Layer on Low Iron Solar Glass. Applied Physics Express, 2013, 6, 032301.	2.4	6
622	Reduction of the efficiency droop in silicon nitride light-emitting devices by localized surface plasmons. Applied Physics Letters, 2013, 102, 081108.	3.3	6
623	Evolution of the sensitized Er3+ emission by silicon nanoclusters and luminescence centers in silicon-rich silica. Nanoscale Research Letters, 2014, 9, 456.	5.7	6
624	Density Functional Theory Study on the Oxidation of Hydrosilylated Silicon Nanocrystals. Journal of Materials Science and Technology, 2014, 30, 639-643.	10.7	6
625	Low-resistivity bulk silicon prepared by hot-pressing boron- and phosphorus-hyperdoped silicon nanocrystals. AIP Advances, 2014, 4, .	1.3	6
626	Ab-initio calculation study on the formation mechanism of boron-oxygen complexes in c-Si. AIP Advances, 2015, 5, .	1.3	6
627	Electrically pumped random lasing with an onset voltage of sub-3 V from ZnO-based light-emitting devices featuring nanometer-thick MoO <sub>3</sub> interlayers. Nanoscale, 2015, 7, 9164-9168.	5.6	6
628	Revealing the elemental-specific growth dynamics of Pt–Cu multipods by scanning transmission electron microscopy and chemical mapping. Journal of Materials Chemistry A, 2015, 3, 21284-21289.	10.3	6
629	Synthesis of colloidal NiO nanocrystals by a hotâ€injection approach with a protecting ligand. Crystal Research and Technology, 2016, 51, 313-317.	1.3	6
630	Aluminum-doped crystalline silicon and its photovoltaic application. Superlattices and Microstructures, 2016, 99, 158-164.	3.1	6

#	Article	IF	CITATIONS
631	Enhanced lithium storage capabilities of NiO@Si core–shell nanowall arrays by voltage-control technique and their use as anode materials for lithium-ion batteries. RSC Advances, 2016, 6, 109649-109656.	3.6	6
632	Characterization of silicon surface states at clean and copper contaminated condition via transient capacitance measurement. Applied Physics Letters, 2017, 111, .	3.3	6
633	Rapid fabrication of porous silicon/carbon microtube composites as anode materials for lithium-ion batteries. RSC Advances, 2018, 8, 41101-41108.	3.6	6
634	Synthesis of Co/SnO2 core-shell nanowire arrays and their electrochemical performance as anodes of lithium-ion batteries. Ionics, 2019, 25, 4651-4658.	2.4	6
635	Litchi-structural core–shell Si@C for high-performance lithium–ion battery anodes. Ionics, 2019, 25, 5809-5818.	2.4	6
636	Investigation on the impact of hydrogen on the passivation of silicon surface states in clean and copper contaminated conditions. AIP Advances, 2019, 9, 105102.	1.3	6
637	Defect control based on constitutional supercooling effect in cast multicrystalline silicon: Boron-indium co-doping. Solar Energy Materials and Solar Cells, 2019, 203, 110189.	6.2	6
638	Effects of nitrogen doping on vacancy-oxygen complexes in neutron irradiated Czochralski silicon. Materials Science in Semiconductor Processing, 2019, 98, 65-69.	4.0	6
639	Light-soaking enhanced passivation of Al2O3 on crystalline silicon surface. Solar Energy Materials and Solar Cells, 2019, 191, 350-355.	6.2	6
640	Influence of temperature gradient at interface on defect multiplication in seed-assisted multicrystalline silicon. Solar Energy Materials and Solar Cells, 2020, 211, 110520.	6.2	6
641	Experimental study of 3D solid-liquid interfaces and their influence on directional solidification silicon ingot. Solar Energy Materials and Solar Cells, 2021, 224, 110991.	6.2	6
642	Electroluminescence from the light-emitting devices with erbium-doped SrTiO3 films on oxidized silicon substrate. Optical Materials, 2021, 119, 111402.	3.6	6
643	Interlayer exciton emission in a MoS <sub>2</sub> /VOPc inorganic/organic van der Waals heterostructure. Materials Horizons, 2022, 9, 1253-1263.	12.2	6
644	The effect and mechanism of current injection to suppress light and elevated temperature induced degradation in p-type cast-mono and multicrystalline silicon Passivated Emitter and Rear cells. Solar Energy, 2022, 235, 12-18.	6.1	6
645	Crystal growth and resistivity modulation of n-type phosphorus-doped cast mono-like silicon. Solar Energy, 2022, 236, 294-300.	6.1	6
646	Doping-dependent nucleation of basal plane dislocations in 4H-SiC. Journal Physics D: Applied Physics, 2022, 55, 334002.	2.8	6
647	Effect of iron on oxygen precipitation in nitrogen-doped Czochralski silicon. Journal of Applied Physics, 1998, 84, 5502-5505.	2.5	5
648	Reduction of oxygen during the crystal growth in heavily antimony-doped Czochralski silicon. Journal of Crystal Growth, 2003, 256, 261-265.	1.5	5

#	Article	IF	CITATIONS
649	Behavior of oxidation-induced stacking faults in annealed Czochralski silicon doped by nitrogen. Journal of Applied Physics, 2003, 93, 8926-8929.	2.5	5
650	Silicon nano-wires grown at low temperature. Physica E: Low-Dimensional Systems and Nanostructures, 2005, 27, 309-313.	2.7	5
651	Effect of nitrogen doping on denuded zone formed by rapid thermal process in Czochralski silicon wafer. Physica B: Condensed Matter, 2006, 376-377, 216-219.	2.7	5
652	Germanium-doped Czochralski silicon: Oxygen precipitates and their annealing behavior. Materials Science in Semiconductor Processing, 2006, 9, 600-605.	4.0	5
653	Stress-dependent transformation of interstitial oxygen in processed Ge-doped Cz-Si. Nuclear Instruments & Methods in Physics Research B, 2006, 253, 205-209.	1.4	5
654	Amorphous SiO x nanowires grown on silicon (100) substrates via rapid thermal process of nanodiamond films. Thin Solid Films, 2006, 503, 18-21.	1.8	5
655	Denuded zone in Czochralski silicon wafer with high carbon content. Journal of Physics Condensed Matter, 2006, 18, 11131-11138.	1.8	5
656	Morphology and phase selective synthesis of EuF3 nanostructures by polyelectrolyte assisted chemical reaction and their optical properties. Materials Chemistry and Physics, 2009, 115, 562-566.	4.0	5
657	Aluminum doped silicon carbide thin films prepared by hot-wire CVD: Influence of the substrate temperature on material properties. Thin Solid Films, 2011, 519, 4516-4518.	1.8	5
658	Performance of Silicon Nanowire Solar Cells with Phosphorus-Diffused Emitters. Journal of Nanomaterials, 2012, 2012, 1-6.	2.7	5
659	Optically and electrically pumped random lasing from ZnO films annealed at different temperatures. Optics Communications, 2012, 285, 5323-5326.	2.1	5
660	Large-scale synthesis of water-soluble Na2SiF6 nanotubes with polyacrylic acid as a surfactant. Materials Research Bulletin, 2012, 47, 3923-3926.	5.2	5
661	Enhancing the photoluminescence intensity of silicon-rich nitride film by localized surface plasmon enhanced photo-excitation. Optics Communications, 2012, 285, 1864-1867.	2.1	5
662	The modulation on luminescence of Er3+-doped silicon-rich oxide films by the structure evolution of silicon nanoclusters. Nanoscale Research Letters, 2013, 8, 34.	5.7	5
663	Temperature dependence of sensitized Er3+ luminescence in silicon-rich oxynitride films. Nanoscale Research Letters, 2014, 9, 489.	5.7	5
664	Twinned silicon and germanium nanocrystals: Formation, stability and quantum confinement. AIP Advances, 2015, 5, .	1.3	5
665	Developing an aqueous approach for synthesizing Au and M@Au (M = Pd, CuPt) hybrid nanostars with plasmonic properties. Physical Chemistry Chemical Physics, 2015, 17, 1265-1272.	2.8	5
666	Impact of carbon co-doping on the performance of crystalline silicon solar cells. Solar Energy Materials and Solar Cells, 2016, 154, 94-98.	6.2	5

#	Article	IF	CITATIONS
667	Electronic and thermoelectric properties of atomically thin C <sub>3</sub> Si <sub>3</sub> /C and C <sub>3</sub> Ge <sub>3</sub> /C superlattices. Nanotechnology, 2018, 29, 045402.	2.6	5
668	Controllable Nitrogen Doping in Multicrystalline Silicon by Casting Under Low Cost Ambient Nitrogen. Silicon, 2018, 10, 1717-1722.	3.3	5
669	Correlation of efficient luminescence with crystal structures of y-Er2Si2O7 and α-Er2Si2O7 in Er-doped silicon oxide films. Journal of Materials Science, 2019, 54, 12668-12675.	3.7	5
670	Unidirectional light scattering by up–down Janus dimers composed of gold nanospheres and silicon nanorods. Optics Communications, 2019, 435, 362-366.	2.1	5
671	Au-Doped intermetallic Pd <sub>3</sub> Pb wavy nanowires as highly efficient electrocatalysts toward the oxygen reduction reaction. CrystEngComm, 2020, 22, 6478-6484.	2.6	5
672	The preparation and characterization of uniform nanoporous structure on glass. Royal Society Open Science, 2020, 7, 192029.	2.4	5
673	Gaâ€Doped Intermetallic Pd3Pb Nanocubes as a Highly Efficient and Durable Oxygen Reduction Reaction Electrocatalyst. ChemistrySelect, 2021, 6, 3891-3896.	1.5	5
674	Facile Synthesis of Pd@PtM (M = Rh, Ni, Pd, Cu) Multimetallic Nanorings as Efficient Catalysts for Ethanol Oxidation Reaction. Frontiers in Chemistry, 2021, 9, 683450.	3.6	5
675	Sensitized electroluminescence from erbium doped silicon rich oxynitride light emitting devices. Journal of Luminescence, 2021, 235, 118009.	3.1	5
676	Enhanced photoluminescence of silicon quantum dots in the presence of both energy transfer enhancement and emission enhancement mechanisms assisted by the double plasmon modes of gold nanorods. Nanoscale Advances, 2021, 3, 4810-4815.	4.6	5
677	Efficient sensitized photoluminescence of Er silicate in silicon oxide films embedded with amorphous silicon clusters, part I: fabrication. Optical Materials Express, 2019, 9, 4329. Nitrogen Decoration of Basal-Plane Dislocations in <mml:math< td=""><td>3.0</td><td>5</td></mml:math<>	3.0	5
678	xmlns:mml="http://www.w3.org/1998/Math/MathML" display="inline" overflow="scroll"> <mml:mn>4</mml:mn> <mml:mrow><mml:mrow><mml:mi mathvariant="normal"&gt;H</mml:mi </mml:mrow></mml:mrow> - <mml:math xmlns:mml="http://www.w3.org/1998/Math/MathML" display="inline"</mml:math 	3.8	5
679	overflow="scroll"> <mml:mi>SiC</mml:mi> . Physical Review Applied, 2022, 17, . Effect of heat treatment on the optical and electrical properties of nitrogen-doped silicon samples. Microelectronic Engineering, 2003, 66, 297-304.	2.4	4
680	Effect of Rapid Thermal Process on Oxygen Precipitation in Heavily Boron-Doped Czochralski Silicon Wafer. Japanese Journal of Applied Physics, 2003, 42, 7290-7291.	1.5	4
681	Grown-in Defects in Heavily Boron-Doped Czochralski Silicon. Japanese Journal of Applied Physics, 2004, 43, 4082-4086.	1.5	4
682	Effect of rapid thermal processing on high temperature oxygen precipitation behaviour in Czochralski silicon wafer. Journal of Physics Condensed Matter, 2004, 16, 3563-3569.	1.8	4
683	Scanning infrared microscopy investigation of copper precipitation in cast multicrystalline silicon. Infrared Physics and Technology, 2006, 47, 240-245.	2.9	4
684	Recombination activity of nickel in Czochralski silicon during rapid thermal process. Materials Science in Semiconductor Processing, 2006, 9, 296-299.	4.0	4

#	Article	IF	CITATIONS
685	Oxygen precipitate denuded zone formation in Czochralski silicon wafer based on rapid thermal processing in nitrogen ambient. Semiconductor Science and Technology, 2007, 22, 1302-1306.	2.0	4
686	Effect of point defects on copper-related deep levels in p-type Czochralski silicon. Journal of Applied Physics, 2007, 102, 073521.	2.5	4
687	A comparison of cathodoluminescence and photoluminescence of porous silicon and the influence of aging and electron irradiation of these properties. Solid State Communications, 2007, 143, 197-201.	1.9	4
688	Effects of defect, carrier concentration and annealing process on the photoluminescence of silicon pn diodes. Materials Science in Semiconductor Processing, 2007, 10, 173-178.	4.0	4
689	Variations of high-pressure thermoelectric and mechanical properties of Si single crystals under doping with N and P–T pre-treatment. Materials Science & Engineering A: Structural Materials: Properties, Microstructure and Processing, 2007, 462, 347-350.	5.6	4
690	Tailor of ZnO morphology by heterogeneous nucleation in the aqueous solution. Materials Research Bulletin, 2007, 42, 1316-1322.	5.2	4
691	Oxygen precipitation in heavily phosphorus-doped silicon wafer annealed at high temperatures. Materials Science and Engineering B: Solid-State Materials for Advanced Technology, 2009, 159-160, 145-148.	3.5	4
692	Electric-field-induced random lasing from ZnO and Mg_01Zn_09O films optically pumped with an extremely low intensity. Optics Express, 2009, 17, 18513.	3.4	4
693	Electrical Transport Properties Through Nanoscale and Large-Area Contacts of ZnO/Si Diodes. Current Nanoscience, 2010, 6, 219-225.	1.2	4
694	Effect of iron contamination on grain boundary states at a direct silicon bonded (110)/(100) interface. Physica Status Solidi - Rapid Research Letters, 2010, 4, 350-352.	2.4	4
695	Defect-Related White-Light Emission from ZnO in an n-Mg0.2Zn0.8O/n-ZnO/SiO x Heterostructure on n-Si. Journal of Electronic Materials, 2010, 39, 652-655.	2.2	4
696	Ultraviolet light emissions from N2 microplasma electrically induced by metal–insulator–semiconductor devices. Journal of Luminescence, 2010, 130, 1073-1075.	3.1	4
697	Modulation of 1.5â€,μm dislocation-related luminescence emitted from a direct silicon bonded interface by external bias. Applied Physics Letters, 2010, 96, 211120.	3.3	4
698	Electrically pumped simultaneous ultraviolet and visible random laser actions from ZnO-CdO interdiffused film. Applied Physics Letters, 2011, 99, 261111.	3.3	4
699	Characterization of a Czochralski grown silicon crystal doped with 10 <sup>20</sup> cm <sup>â€3</sup> germanium. Crystal Research and Technology, 2011, 46, 10-13.	1.3	4
700	Surface plasmon enhanced light emission of silicon-rich silicon nitride: Dependence on metal island size. Applied Surface Science, 2011, 257, 5591-5594.	6.1	4
701	Investigation of nitrogen behaviors during Czochralski silicon crystal growth. Journal of Crystal Growth, 2011, 318, 178-182.	1.5	4
702	The origin of 0.78 eV line of the dislocation related luminescence in silicon. Journal of Applied Physics, 2012, 112, .	2.5	4

#	Article	IF	CITATIONS
703	Effect of Ge doping on the kinetics of iron–boron pair association and dissociation in photovoltaic silicon. Journal of Crystal Growth, 2012, 348, 20-24.	1.5	4
704	Crystal Growth of Indium-Doped Czochralski Silicon for Photovoltaic Application. Japanese Journal of Applied Physics, 2012, 51, 105501.	1.5	4
705	Density functional theory study of the impact of tin doping on oxygen diffusion in Czochralski silicon. Physica Status Solidi (A) Applications and Materials Science, 2013, 210, 2199-2203.	1.8	4
706	Analysis of the photovoltaic properties of n-type compensated silicon solar cells with the Al-alloyed emitter. Journal of Alloys and Compounds, 2013, 561, 28-32.	5.5	4
707	Room temperature visible electroluminescence from SrTiO3/p+–Si heterostructure. Scripta Materialia, 2013, 69, 748-751.	5.2	4
708	Electrically pumped random lasing from the light-emitting device based on two-fold-tandem SiO2/ZnO structure. Applied Physics Letters, 2013, 102, 161112.	3.3	4
709	Size-dependent coupling between localized surface plasmons and excitons in silicon nitride matrix. Optics Letters, 2013, 38, 2832.	3.3	4
710	Scanning infrared microscopy study of thermal processing induced defects in low resistivity Si wafers. Semiconductor Science and Technology, 2013, 28, 085013.	2.0	4
711	Low temperature iron gettering by grown-in defects in p-type Czochralski silicon. Superlattices and Microstructures, 2016, 99, 192-196.	3.1	4
712	Defect-related electroluminescence from metal-oxide-semiconductor devices with ZrO2 films on silicon. Superlattices and Microstructures, 2016, 99, 186-191.	3.1	4
713	Inhomogeneous composition distribution in monolayer transition metal dichalcogenide alloys. Materials Research Express, 2017, 4, 045004.	1.6	4
714	Formation kinetics and mechanism of metastable vacancy-dioxygen complex in neutron irradiated Czochralski silicon. Superlattices and Microstructures, 2017, 107, 91-96.	3.1	4
715	Size-controlled synthesis of Au nanorings on Pd ultrathin nanoplates as efficient catalysts for hydrogenation. CrystEngComm, 2017, 19, 6588-6593.	2.6	4
716	Effect of germanium doping on the formation kinetics of vacancy-dioxygen complexes in high dose neutron irradiated crystalline silicon. Journal of Applied Physics, 2017, 122, 095704.	2.5	4
717	Detailed study of SiOxNy:H/Si interface properties for high quality surface passivation of crystalline silicon. Superlattices and Microstructures, 2018, 113, 13-19.	3.1	4
718	Enhanced oxygen reduction activity of Pt shells on PdCu truncated octahedra with different compositions. RSC Advances, 2018, 8, 34853-34859.	3.6	4
719	Effects of Iron Contamination and Hydrogen Passivation on the Electrical Properties of Oxygen Precipitates in CZ-Si. Journal of Electronic Materials, 2018, 47, 5039-5044.	2.2	4
720	Building a Bridge from Papermaking to Solar Fuels. Angewandte Chemie, 2019, 131, 14992-14996.	2.0	4

#	Article	IF	CITATIONS
721	Recombination activity of sub-grain boundaries and dislocation arrays in quasi-single crystalline silicon. Applied Physics Express, 2019, 12, 051012.	2.4	4
722	Microdefect Characteristics in Castâ€Mono Silicon Wafers Induced by Slurry Sawing. Physica Status Solidi (A) Applications and Materials Science, 2021, 218, 2000258.	1.8	4
723	Technoeconomically competitive four-terminal perovskite/graphene-silicon tandem solar cells with over 20% efficiency. Journal of Energy Chemistry, 2021, 63, 477-483.	12.9	4
724	Facile Synthesis of PdCuRu Porous Nanoplates as Highly Efficient Electrocatalysts for Hydrogen Evolution Reaction in Alkaline Medium. Metals, 2021, 11, 1451.	2.3	4
725	Evaluation of large-scale recycled seed for cast monocrystalline silicon: Defect multiplication mechanisms and feasibility. Solar Energy Materials and Solar Cells, 2021, 230, 111266.	6.2	4
726	Confinement effect and low-defect density-induced long lifetime Er silicate nanowire embedded in silicon oxide film. Optics Express, 2020, 28, 13216.	3.4	4
727	Improved Efficiency for Siliconâ€Based Perovskite Lightâ€Emitting Diodes via Interfacial Hydrophilic Modification. Advanced Materials Interfaces, 2021, 8, 2101448.	3.7	4
728	Hyperdoped Crystalline Silicon for Infrared Photodetectors by Pulsed Laser Melting: A Review. Physica Status Solidi (A) Applications and Materials Science, 2022, 219, .	1.8	4
729	The impact of nitrogen on power diode characteristics. Materials Science and Engineering B: Solid-State Materials for Advanced Technology, 2002, 91-92, 495-497.	3.5	3
730	Effect of oxygen precipitation on voids in bulk silicon. Microelectronic Engineering, 2003, 66, 289-296.	2.4	3
731	Bipolar Structure in Thermally Treated Czochralski Silicon Wafer. Japanese Journal of Applied Physics, 2003, 42, 1129-1132.	1.5	3
732	Extended defects in nitrogen-doped Czochralski silicon during diode process. Physica B: Condensed Matter, 2004, 348, 226-230.	2.7	3
733	Synthesis and characterization of CdS based sulfide coaxial cable and nanotubes by sacrificial approach. Materials Letters, 2006, 60, 2004-2008.	2.6	3
734	Rapid-thermal-processing-based internal gettering for heavily boron-doped Czochralski silicon. Journal of Applied Physics, 2006, 100, 103530.	2.5	3
735	Electroluminescent and carrier transport mechanisms of MgxZn1â^'xOâ^•Si heterojunctions. Journal of Applied Physics, 2007, 102, 083106.	2.5	3
736	Study of photoconductivity and photoluminescence of organic/porous silicon complexes. Applied Surface Science, 2007, 253, 4566-4569.	6.1	3
737	Effect of point defects on the recombination activity of copper precipitates in p-type Czochralski silicon. Journal of Materials Science: Materials in Electronics, 2008, 19, 32-35.	2.2	3
738	Enhanced oxygen diffusion in Czochralski silicon at 450–650 °C. Physica Status Solidi (A) Applications and Materials Science, 2008, 205, 1148-1151.	1.8	3

#	Article	IF	CITATIONS
739	Electron-beam-induced current evidence for room-temperature photoluminescence of silicon pn diode. Vacuum, 2008, 82, 1337-1340.	3.5	3
740	Effect of annealing atmosphere on the recombination activity of copper precipitates formed by rapid thermal process in conventional and nitrogen-doped Czochralski silicon wafers. Journal of Applied Physics, 2008, 103, 014912.	2,5	3
741	Electroluminescence of silicon-rich silicon nitride light-emitting devices. , 2008, , .		3
742	Grown-in defects in heavily phosphorus-doped Czochralski silicon. Physica B: Condensed Matter, 2009, 404, 4619-4621.	2.7	3
743	Iron precipitation in as-received Czochralski silicon during low temperature annealing. Materials Science in Semiconductor Processing, 2009, 12, 185-188.	4.0	3
744	Effect of nickel contamination on grain boundary states at a direct silicon bonded (1 1 0)/(1 0 0) interface. Scripta Materialia, 2010, 63, 1100-1103.	5.2	3
745	Phosphorus gettering of precipitated Cu in single crystalline silicon based on rapid thermal process. Journal of Crystal Growth, 2010, 312, 3069-3074.	1.5	3
746	Influence of nickel precipitation on the formation of denuded zone in Czochralski silicon. Journal of Alloys and Compounds, 2010, 502, 351-355.	5.5	3
747	Si <sub>60</sub> fullerene-like cage passivated by F and Cl. Molecular Simulation, 2010, 36, 493-495.	2.0	3
748	Hydrogen passivation of Fe-related deep energy levels at a direct silicon-bonded (110)/(100) grain boundary. Scripta Materialia, 2011, 64, 653-656.	5.2	3
749	Formation of shallow junctions in gallium and phosphorus compensated silicon for cell performance improvement. Scripta Materialia, 2011, 65, 871-874.	5.2	3
750	Direct synthesis of indium nanoparticles and their application to prepare CuInS2 thin films and solar cells. Journal of Sol-Gel Science and Technology, 2011, 58, 162-169.	2.4	3
751	Flow pattern defects in germanium-doped Czochralski silicon crystals. Applied Physics A: Materials Science and Processing, 2011, 104, 349-355.	2.3	3
752	Shape and size controlled synthesis of CuInS2 particles in polyalcohol system used as "printable ink― for thin films. Journal of Sol-Gel Science and Technology, 2012, 62, 87-91.	2.4	3
753	An etchant for delineation of flow pattern defects in heavily doped p-type silicon wafers. Materials Science in Semiconductor Processing, 2013, 16, 893-898.	4.0	3
754	Enhancement of orange-yellow electroluminescence extraction from SiNx light-emitting devices by silver nanostructures. Optics Express, 2013, 21, 846.	3.4	3
755	Optimization of the electroluminescence from SiNx-based light-emitting devices by modulating the size and morphology of silver nanostructures. Optics Express, 2013, 21, 1675.	3.4	3
756	Oxide precipitate nucleation at 300 °C in low resistivity n-type Czochralski Si. Physica Status Solidi (A) Applications and Materials Science, 2013, 210, 2592-2599.	1.8	3

#	Article	IF	CITATIONS
757	Enhanced broadband light absorption in silicon film by large-size lumpy silver particles. Applied Physics A: Materials Science and Processing, 2014, 117, 573-577.	2.3	3
758	Generation kinetics of boron-oxygen complexes in p-type compensated c-Si. Applied Physics Letters, 2014, 104, 102108.	3.3	3
759	Room-Temperature Near-Infrared Electroluminescence from Boron-Diffused Silicon Pn-Junction Diodes. Frontiers in Materials, 2015, 2, .	2.4	3
760	Photoelectric properties of reduced-graphene-oxide film and its photovoltaic application. RSC Advances, 2015, 5, 39630-39634.	3.6	3
761	Cobalt Oxide–Tin Core–Shell Nanowire Arrays as Highâ€Performance Electrodes for Lithiumâ€Ion Batteries. Energy Technology, 2016, 4, 1435-1439.	3.8	3
762	Impact of germanium co-doping on oxygen precipitation in heavily boron-doped Czochralski silicon. Superlattices and Microstructures, 2016, 99, 35-40.	3.1	3
763	Multistage Transformation and Lattice Fluctuation at AgCl–Ag Interface. Journal of Physical Chemistry Letters, 2017, 8, 5853-5860.	4.6	3
764	Cobalt Oxide@Tin Oxide@Silver Core–Shell Nanowire Arrays as Electrodes for Lithiumâ€Ion Batteries. Energy Technology, 2017, 5, 277-282.	3.8	3
765	The devisable reflection-enhanced lumpy silver particle and its application in thin film amorphous silicon solar cell. Journal of Materials Science: Materials in Electronics, 2018, 29, 3153-3159.	2.2	3
766	Fabrication of stabilized and dispersive copper nanowires ink. Journal of Materials Science: Materials in Electronics, 2018, 29, 14989-14994.	2.2	3
767	An Innovative Light Trapping Structure Fabrication Method on Diamondâ€Wireâ€Sawing Multiâ€Crystalline Silicon Wafers. ChemistrySelect, 2018, 3, 7561-7564.	1.5	3
768	Simulation to confirm the existence of distinct low-temperature regions in a Si melt using an insulating plate under the crucible bottom for the noncontact crucible method. Journal of Crystal Growth, 2019, 524, 125160.	1.5	3
769	Optimized phosphorus diffusion process and performance improvement of c-Si solar cell by eliminating SiP precipitates in the emitter. Journal of Materials Science: Materials in Electronics, 2019, 30, 13820-13825.	2.2	3
770	Revisiting the effects of carbon-doping at 1017Âcmâ^'3 level on dislocation behavior of Czochralski silicon: from room temperature to elevated temperatures. Journal of Materials Science: Materials in Electronics, 2019, 30, 3114-3123.	2.2	3
771	Effects of Antimony- and Tin-Doping on the Mechanical Propertiesof Czochralski Silicon: Revealing the Role of Electrical Activity of Antimony. Silicon, 2020, 12, 1433-1439.	3.3	3
772	Improving CdTeâ€Based Thinâ€Film Solar Cell Efficiency with the Oxygenated CdSe Layer Prepared by Sputtering Process. Physica Status Solidi (A) Applications and Materials Science, 2020, 217, 2000560.	1.8	3
773	Effects of vacancy defects on the mechanical properties in neutron irradiated Czochralski silicon. Journal of Physics Condensed Matter, 2020, 32, 275702.	1.8	3
774	On the mechanism underlying the elimination of nitrogen-oxygen shallow thermal donors in nitrogen-doped Czochralski silicon at elevated temperatures. Journal of Applied Physics, 2021, 129, .	2.5	3

#	Article	IF	CITATIONS
775	Performance Improvement of Galliumâ€Doped Passivated Emitter and Rear Cells by Twoâ€Step Bias Application. Solar Rrl, 0, , 2100738.	5.8	3
776	Effects of co-doping nitrogen and germanium on dislocation gliding in Czochralski silicon: Implication for improving mechanical strength. Journal of Applied Physics, 2020, 128, 235105.	2.5	3
777	A New Design of Side Heater for 3D Solid-liquid Interface Improvement in G8 Directional Solidification Silicon Ingot Growth. Silicon, 2022, 14, 9407-9416.	3.3	3
778	Efficient Sensitized Photoluminescence from Erbium Chloride Silicate via Interparticle Energy Transfer. Materials, 2022, 15, 1093.	2.9	3
779	Facile synthesis of PdSn alloy octopods through the Stranski–Krastanov growth mechanism as electrocatalysts towards the ethanol oxidation reaction. CrystEngComm, 2022, 24, 3230-3238.	2.6	3
780	Influence of Dislocations on Nitrogen–Oxygen Complex in Silicon. Physica Status Solidi A, 1999, 171, 203-207.	1.7	2
781	Electrical Activity of Nitrogen-Oxygen Complexes in Silicon. Physica Status Solidi (B): Basic Research, 2000, 221, 641-645.	1.5	2
782	Oxygen precipitation in Czochralski silicon annealed at 450°C under a high pressure of 1GPa. Physica B: Condensed Matter, 2003, 327, 60-64.	2.7	2
783	Dislocation Formation in Czochralski Si Crystal Growth Using an Annealed Heavily B-Doped Si Seed. Japanese Journal of Applied Physics, 2003, 42, L1299-L1301.	1.5	2
784	Blue emission of porous silicon intensified by boron deposition. Journal of Materials Science, 2005, 40, 5071-5073.	3.7	2
785	Enhancement of oxygen precipitation in Czochralski silicon wafers by high-temperature anneals. Physica B: Condensed Matter, 2006, 376-377, 169-172.	2.7	2
786	Crystal growth and oxygen precipitation behavior of 300mm nitrogen-doped Czochralski silicon. Journal of Crystal Growth, 2006, 292, 257-259.	1.5	2
787	One-dimensional silicon nanostructures fabricated by thermal evaporation. Materials Science and Engineering C, 2006, 26, 800-804.	7.3	2
788	Effect of Nitrogen Doping on Oxygen Precipitate Profiles in Czochralski Silicon Wafer. Japanese Journal of Applied Physics, 2006, 45, 4903-4907.	1.5	2
789	Evolution of nitrogen pairs and nitrogen-oxygen complexes in nitrogen-doped Czochralski silicon. Physica Status Solidi C: Current Topics in Solid State Physics, 2007, 4, 3090-3094.	0.8	2
790	Copper precipitation in nitrogen-doped Czochralski silicon. Journal of Applied Physics, 2008, 104, 013508.	2.5	2
791	Oxygen precipitation in heavily phosphorus-doped Czochralski silicon: effect of nitrogen codoping. Semiconductor Science and Technology, 2009, 24, 105030.	2.0	2
792	Internal gettering for germanium-doped Czochralski silicon: Treated by rapid-thermal-anneal based processing simulation. Materials Science and Engineering B: Solid-State Materials for Advanced Technology, 2009, 159-160, 235-238.	3.5	2

#	Article	IF	CITATIONS
793	Enhancement effect of nitrogen co-doping on oxygen precipitation in heavily phosphorus-doped Czochralski silicon during high-temperature annealing. Journal of Crystal Growth, 2009, 311, 3273-3277.	1.5	2
794	Correlation Between Oxygen Precipitation and Extended Defects in Czochralski Silicon: Investigation by Means of Scanning Infrared Microscopy. Journal of Electronic Materials, 2010, 39, 648-651.	2.2	2
795	Fairly pure ultraviolet electroluminescence from p-Si-based SiOx/ZnO/SiOx double-barrier device. Optics Communications, 2010, 283, 1359-1362.	2.1	2
796	Oxygen Precipitate Nucleation in Heavily Antimony-Doped Czochralski Silicon. ECS Transactions, 2010, 27, 1027-1033.	0.5	2
797	Continuous wave spectroscopy of nonlinear dynamics of Si nanocrystals in a microdisk resonator. Physical Review B, 2011, 84, .	3.2	2
798	Influence of oxygen precipitation on copper precipitation in Czochralski silicon. Journal of Applied Physics, 2012, 111, 094907.	2.5	2
799	Retarded oxygen diffusion in heavily phosphorus-doped Czochralski silicon: experiments and first-principles calculations. Journal of Physics Condensed Matter, 2012, 24, 495802.	1.8	2
800	Dislocation-induced variation of generation kinetics of boron–oxygen complexes in silicon. Journal of Crystal Growth, 2012, 359, 69-71.	1.5	2
801	Hydrogenation of interface states at a clean grain boundary in the direct silicon bonded wafer. Physica Status Solidi (A) Applications and Materials Science, 2012, 209, 990-993.	1.8	2
802	Phosphorus diffusion gettering of substitutional metal contaminants at a small-angle grain boundary in n-type silicon: The case of gold. Journal of Crystal Growth, 2013, 380, 51-54.	1.5	2
803	Electrically pumped random lasing in ZnO-based metal-insulator-semiconductor structured devices: Effect of ZnO film thickness. Journal of Applied Physics, 2013, 113, 213103.	2.5	2
804	Modulation of electrical characteristics at a Ni-contaminated silicon grain boundary by engineering the metal precipitates. Physica Status Solidi (A) Applications and Materials Science, 2013, 210, 1828-1831.	1.8	2
805	Boron deactivation in heavily boron-doped Czochralski silicon during rapid thermal anneal: Atomic level understanding. Applied Physics Letters, 2014, 104, 032102.	3.3	2
806	Visible and near-infrared electroluminescence from TiO2/p+-Si heterostructured device. AIP Advances, 2014, 4, 047109.	1.3	2
807	Silicon Nanocrystals: Sizeâ€Đependent Structures and Optical Absorption of Boronâ€Hyperdoped Silicon Nanocrystals (Advanced Optical Materials 5/2016). Advanced Optical Materials, 2016, 4, 646-646.	7.3	2
808	Cu-Li2O@Si core-shell nanowall arrays: Facile voltage-controlled synthesis and enhanced lithium-storage capabilities. Journal of Alloys and Compounds, 2016, 689, 56-62.	5.5	2
809	Oxygen Reduction Reaction: Tuning Surface Structure and Strain in Pd–Pt Core–Shell Nanocrystals for Enhanced Electrocatalytic Oxygen Reduction (Small 7/2017). Small, 2017, 13, .	10.0	2
810	Impact of Carbon Codoping on Generation and Dissociation of Boron–Oxygen Defects in Czochralski Silicon. Journal of Electronic Materials, 2018, 47, 5092-5098.	2.2	2

#	Article	lF	CITATIONS
811	Flash Solid–Solid Synthesis of Silicon Oxide Nanorods. Small, 2020, 16, 2001435.	10.0	2
812	Evolution from random lasing to erbium-related electroluminescence from metal-insulator-semiconductor structured light-emitting device with erbium-doped ZnO film on silicon. Journal of Applied Physics, 2020, 127, .	2.5	2
813	Effect of oxygen concentration on minority carrier lifetime at the bottom of quasi-single crystalline silicon. Materials Science in Semiconductor Processing, 2021, 123, 105497.	4.0	2
814	Role of metal impurities in multicrystalline silicon solar cell degradation. Applied Physics Express, 2021, 14, 115502.	2.4	2
815	Nitrogen Impurity in Crystalline Silicon. , 2019, , 463-494.		2
816	Comprehensive understanding on germanium-doping effects on oxygen precipitation in Czochralski silicon wafers with a prior rapid thermal anneal. Applied Physics A: Materials Science and Processing, 2021, 127, 1.	2.3	2
817	Carrier injection and annealing enhanced electrical performance in tunnel oxide passivated contact silicon solar cells. Physica Status Solidi (A) Applications and Materials Science, 0, , 2100614.	1.8	2
818	Electroluminescence from light-emitting device with erbium-doped TiO2 film sputtered onp+-Si substrate: Enhancement effect of codoping zirconium. Thin Solid Films, 2022, 748, 139160.	1.8	2
819	Investigation of thermal donors in Czochralski silicon annealed at 450°C under high pressure of 1GPa. Physica B: Condensed Matter, 2003, 339, 204-207.	2.7	1
820	Effect of oxygen precipitates and induced dislocations on oxidation-induced stacking faults in nitrogen-doped Czochralski silicon. Journal of Applied Physics, 2004, 96, 3031-3033.	2.5	1
821	Microstructure of high temperature–pressure treated nitrogen-doped Czochralski silicon. Journal of Alloys and Compounds, 2004, 382, 275-277.	5.5	1
822	Effects of rapid thermal processing on oxide precipitation in conventional and nitrogen-doped Czochralski silicon. Physica Status Solidi (A) Applications and Materials Science, 2006, 203, 670-676.	1.8	1
823	Stress dependent structure of annealed nitrogen-doped Cz-Si. Materials Science and Engineering B: Solid-State Materials for Advanced Technology, 2006, 134, 218-221.	3.5	1
824	Nitrogen-doped Czochralski silicon treated in rapid thermal process. Materials Science and Engineering B: Solid-State Materials for Advanced Technology, 2006, 134, 193-201.	3.5	1
825	Blue light emission of porous silicon subjected to RTP treatments. Science Bulletin, 2006, 51, 2696-2699.	1.7	1
826	STUDY OF OPTICAL PROPERTIES OF POROUS SILICON PRODUCED BY METAL-AID. Modern Physics Letters B, 2007, 21, 1989-1997.	1.9	1
827	Diamond nanocrystals and amorphous SiOx nanowires formed by rapid thermal annealing of carbon film. Thin Solid Films, 2007, 515, 6707-6712.	1.8	1
828	Recombination activity of nickel in nitrogen-doped Czochralski silicon treated by rapid thermal processing. Materials Science in Semiconductor Processing, 2007, 10, 222-226.	4.0	1

#	Article	IF	CITATIONS
829	Dissolution of oxygen precipitates in germanium-doped Czochralski silicon during rapid thermal annealing. Journal of Crystal Growth, 2007, 308, 247-251.	1.5	1
830	Effect of rapid thermal treatment on photoluminescence of surface passivated porous silicon. Journal of Luminescence, 2008, 128, 317-320.	3.1	1
831	Oxygen Precipitation in Heavily Phosphorus-doped Czochralski Silicon. ECS Transactions, 2009, 18, 1001-1011.	0.5	1
832	High temperature nucleation of oxygen precipitates in Germanium-doped Czochralski silicon. Thin Solid Films, 2010, 518, 2334-2337.	1.8	1
833	Electrically pumped wavelength-tunable blue random lasing from CdZnO films on silicon. Applied Physics Letters, 2012, 100, 231101.	3.3	1
834	An Etchant for Delineation of Flow Pattern Defects in Heavily Doped n-type Silicon Wafers. ECS Transactions, 2012, 44, 751-757.	0.5	1
835	Anomalous Magnetization Behavior of Fe-N Films Deposited by Reactive Pulsed Laser Deposition. IEEE Transactions on Magnetics, 2012, 48, 2899-2902.	2.1	1
836	Defects in TiO2 films on p+-Si studied by positron annihilation spectroscopy. Materials Science and Engineering B: Solid-State Materials for Advanced Technology, 2012, 177, 625-628.	3.5	1
837	Iron-boron pair dissociation in silicon under strong illumination. AIP Advances, 2013, 3, .	1.3	1
838	Structural and luminescent properties of electron-irradiated silicon. , 2014, , .		1
839	Enhanced internal gettering in n/n+ epitaxial silicon wafer: coaction of nitrogen impurity and vacancy on oxygen precipitation in substrate. Journal of Materials Science: Materials in Electronics, 2014, 25, 3486-3491.	2.2	1
840	Investigating the Effect of Thermal Annealing Process on the Photovoltaic Performance of the Graphene-Silicon Solar Cell. International Journal of Photoenergy, 2015, 2015, 1-6.	2.5	1
841	Effect of Dopant Compensation on the Behavior of Dissolved Iron and Iron-Boron Related Complexes in Silicon. International Journal of Photoenergy, 2015, 2015, 1-6.	2.5	1
842	Graphene Quantum Dots: Highly Pure and Luminescent Graphene Quantum Dots on Silicon Directly Grown by Chemical Vapor Deposition (Part. Part. Syst. Charact. 1/2016). Particle and Particle Systems Characterization, 2016, 33, 2-2.	2.3	1
843	Graphene coupled with silicon quantum dots for high-performance silicon Schottky photodetectors. , 2016, , .		1
844	Thermal history effect on the nucleation of oxygen precipitates in germanium doped Cz-silicon studied by high-energy X-ray diffraction. Journal of Crystal Growth, 2017, 479, 46-51.	1.5	1
845	Density functional theory study on the boron and phosphorus doping of germanium quantum dots. RSC Advances, 2017, 7, 50935-50941.	3.6	1
846	Carbon effect on the survival of vacancies in Czochralski silicon during rapid thermal anneal. Journal of Applied Physics, 2017, 122, 045705.	2.5	1

#	Article	IF	CITATIONS
847	Effect of Smallâ€Angle Grain Boundary on the Mechanical Properties in Direct Silicon Bonded Wafer. Physica Status Solidi (A) Applications and Materials Science, 2018, 215, 1800118.	1.8	1
848	Hydrogen passivation of iron-acceptor pairs in boron and gallium co-doped crystalline silicon. Applied Physics Express, 2020, 13, 011002.	2.4	1
849	A microscopic TEM study of the defect layers in cast-mono crystalline silicon wafers induced by diamond-wire sawing. AIP Advances, 2021, 11, 045103.	1.3	1
850	Effect of prior stress-relief on the gliding of indentation dislocations on silicon wafers. Wuli Xuebao/Acta Physica Sinica, 2015, 64, 208101.	0.5	1
851	Growth of Crystalline Silicon for Solar Cells: Czochralski Si. , 2017, , 1-45.		1
852	Growth of Crystalline Silicon for Solar Cells: Czochralski Si. , 2019, , 129-174.		1
853	Kick-out diffusion of Al in 4H-SiC: an <i>ab initio</i> study. Journal of Applied Physics, 2022, 132, .	2.5	1
854	Oxygen precipitation kinetics of Czochralski silicon preannealed under high pressure. Physica B: Condensed Matter, 2003, 340-342, 1041-1045.	2.7	0
855	Bipolar structure of carrier concentration in hydrogen pre-annealing Czochralski silicon wafer. Physica B: Condensed Matter, 2003, 340-342, 601-604.	2.7	0
856	Defect engineering in silicon used for ultra large-scale integrated circuits. , 0, , .		0
857	Effect of ramping anneals under inert or oxidizing ambient on the formation of oxygen precipitate denuded zone in nitrogen-doped Czochralski silicon wafers. Physica Status Solidi (A) Applications and Materials Science, 2006, 203, 1934-1939.	1.8	0
858	Preface: phys. stat. sol. (a) 203/4. Physica Status Solidi (A) Applications and Materials Science, 2006, 203, 657-658.	1.8	0
859	Effects of two-step rapid thermal processing in different ambients on denuded zone and oxygen precipitation in Czochralski silicon. Physica Status Solidi C: Current Topics in Solid State Physics, 2007, 4, 3080-3085.	0.8	0
860	Effect of vacancies on copper precipitation in nâ€ŧype Czochralski silicon. Physica Status Solidi (A) Applications and Materials Science, 2008, 205, 2662-2665.	1.8	0
861	Hydrofluoric acid free synthesis of macropores on silicon by chemical vapor deposition and their photoluminescence. Physica E: Low-Dimensional Systems and Nanostructures, 2008, 40, 494-498.	2.7	0
862	Impurity effect on internal gettering in Czochralski silicon. , 2008, , .		0
863	Photoluminescence enhancement of Silicon-rich silicon nitride film induced by silver localized surface plasmon. , 2008, , .		0
864	Intense photoluminescence from Eu-doped silicon-rich silicon oxide films prepared by electron beam evaporation. , 2009, , .		0

#	Article	IF	CITATIONS
865	Surface plasmon enhanced electroluminescence of SiNx film based MIS device. , 2010, , .		0
866	Quantum dots decorated single walled carbon nanotubes for multimodal cellular imaging. , 2010, , .		0
867	Photoluminescence from dislocations in silicon induced by irradiation of electron beams. , 2010, , .		0
868	Internal gettering of copper contamination in Czochralski silicon. , 2010, , .		0
869	Electrically pumped random lasing from ZnO materials. , 2010, , .		0
870	The improvement effect of carrier injection by Ag nanoparticles on the electroluminescence of SiN <inf>x</inf> -based LEDs. , 2012, , .		0
871	Study of sulphidation of Cu–In nanoparticle precursor films with an air-stable process. Journal of Materials Science: Materials in Electronics, 2012, 23, 1263-1267.	2.2	0
872	Effect of scattering from localized surface plasmon resonance on improving the luminescence efficiency of silicon nitride light-emitting devices. Journal of Nanoparticle Research, 2013, 15, 1.	1.9	0
873	Boron-Phosphorus Pairs in Compensated Crystalline Silicon. ECS Solid State Letters, 2014, 3, N23-N25.	1.4	0
874	On the mechanism of carrier scattering at oxide precipitates in Czochralski silicon. Journal of Materials Science: Materials in Electronics, 2015, 26, 2589-2594.	2.2	0
875	Rapid thermal processing induced vacancy-oxygen complexes in Czochralski-grown Si1â^'xGex. Journal of Materials Science: Materials in Electronics, 2015, 26, 7666-7672.	2.2	0
876	Silver nanoshells plasmonically controlled random lasing without dielectric spacer. , 2015, , .		0
877	Defect-Related Electroluminescence in the 1.2–1.7Âμm Range from Boron-Implanted Silicon at Room Temperature. Journal of Electronic Materials, 2018, 47, 4970-4974.	2.2	0
878	Frontispiece: Building a Bridge from Papermaking to Solar Fuels. Angewandte Chemie - International Edition, 2019, 58, .	13.8	0
879	Frontispiz: Building a Bridge from Papermaking to Solar Fuels. Angewandte Chemie, 2019, 131, .	2.0	0
880	Kinetic suppression of boron–oxygen complexes in p-type Czochralski silicon by tin doping. Applied Physics Express, 2019, 12, 011005.	2.4	0
881	Oxygen precipitation in Ge-doped Czochralski-silicon at 900 °C investigated by <i>in situ</i> high energy x-ray diffraction. AIP Advances, 2020, 10, .	1.3	0
882	(Invited) Defects in Cast-Mono Crystalline Silicon. ECS Meeting Abstracts, 2021, MA2021-01, 1090-1090.	0.0	0

#	Article	IF	CITATIONS
883	Effects of dopants on the growth of oxidation-induced stacking faults in heavily doped n-type Czochralaki silicon. Wuli Xuebao/Acta Physica Sinica, 2015, 64, 096105.	0.5	Ο
884	Nitrogen Impurity in Crystalline Silicon. , 2019, , 1-32.		0
885	Efficient sensitized photoluminescence of Er silicate in silicon oxide films embedded with amorphous silicon clusters, part II: photoluminescence. Optical Materials Express, 2019, 9, 4339.	3.0	0
886	Effect of Germanium Codoping on the Grownâ€In Oxide Precipitates in Nitrogenâ€Doped Czochralski Silicon. Physica Status Solidi (A) Applications and Materials Science, 2022, 219, .	1.8	0
887	Participation of nitrogen impurities in the growth of grown-in oxide precipitates in nitrogen-doped Czochralski silicon. Journal of Applied Physics, 2022, 131, 155703.	2.5	0